University of Alberta

Two Dimensional Modelling of Volatile Organic Compounds Adsorption in a Fixed Bed Adsorber

by

Dereje Tamiru Tefera

A thesis submitted to the Faculty of Graduate Studies and Research

in partial fulfillment of the requirements for the degree of

Master of Science

in

Environmental Engineering

Civil and Environmental Engineering

Fall 2013

Edmonton, Alberta

Abstract

In this research two-dimensional mathematical models were developed to study adsorption of single component volatile organic compounds (VOCs) and competitive adsorption of n-component mixtures of VOCs from dilute gas streams in a fixed-bed adsorber. The models consist of the macroscopic mass, energy and momentum conservation equations and isotherm equations. Langmuir isotherm was used for single component VOC adsorption, while a new multicomponent isotherm model was derived to predict adsorption equilibria of VOCs mixture from single component isotherm data. The models were validated with experiments wherein deviation between measured and modeled data was quantified using the mean absolute relative error (MARE).

The single component adsorption model predicted the breakthrough curves of the tested VOCs (acetone, benzene, toluene and 1, 2, 4-trimethylbenzene as well as the pressure drop and temperature during benzene adsorption with MRAE of 2.6, 11.8, and 0.8%, respectively. The model also showed very good sensitivity to the changes in operations variables such as temperature and superficial velocity of the carrier gas, channeling, and adsorbent particle size. The competitive adsorption model predicted the breakthrough profiles of binary and eight-component VOCs mixtures with 13 and 12%, MRAE respectively while that of the adsorbed amounts was 1 and 2%, respectively. These results indicate the accuracy of the models to simulate a fixed bed adsorber and their potential to be used for enhancing absorber design and optimization.

Acknowledgements

First and foremost I would like to express my sincere debt of gratitude to my supervisor, Dr. Zaher Hashisho, for his dedication to the research, expertise, supervision, and encouragement extended to me throughout my course work and research. Dr. Zaher Hashisho's support, guidance and valuable comments during the thesis and paper writing are also greatly appreciated. I consider it an honor to work with you.

Secondly I would like to acknowledge financial support for this research from Ford Motor Company and the Natural Science and Engineering Research Council (NSERC) of Canada. I also acknowledge the support of infrastructure and instruments grants from Canada Foundation for Innovation (CFI), NSERC, and Alberta Advanced Education and Technology.

Third, I would like to show my appreciation to the technical support staffs of the Civil and Environmental Engineering Department at the University of Alberta: Dale Lathe, Elena Dlusskaya and Chen Liang for their assistance and cooperation during the research**.**

I also thank my fellows in the Air Quality Characterization and Control Lab for their cooperation.

Finally I would like to thank my family, friends and anyone who directly or indirectly have lent their helping hands in this venture.

Table of Contents

List of Tables

List of Figures

CHAPTER 1 INTRODUCTION

1.1 Background

The definition of volatile organic compound (VOCs) varies among regulatory systems depending on whether the emphasis is on their impact to the environment or directly to human health. For example the United states Environmental Protection Agency (USEPA) defines VOC as "any compound of carbon, excluding carbon monoxide, carbon dioxide, carbonic acid, metallic carbides or carbonates, and ammonium carbonate, which participates in atmospheric photochemical reactions" [1]. The Canadian Environmental Protection Act (CEPA) on the other hand, giving emphasis to commonly encountered VOCs that would have an effect on air quality, defines VOCs as "carbon-containing gases and vapors such as gasoline fumes and solvents excluding carbon dioxide, carbon monoxide, methane, and chlorofluorocarbons" [2]. The World Health Organisation defines VOC as any organic compound whose boiling point is in the range from (50-100°C) to (240-260°C) [3] and the European Union on defines VOC as "any organic compound having an initial boiling point less than or equal to 250 °C measured at a standard atmospheric pressure of 101.3 kPa and can do damage to visual or audible senses" [2]. The last definition seems to include most VOCs of environmental concern and those that have direct health effect on human beings.

VOCs are emitted to the atmosphere from natural (biogenic) and anthropogenic sources. Natural sources of VOCs include forests, wetlands, oceans and volcanoes [4]. The most common anthropogenic sources of VOCs are vehicular emission, chemical manufacturing facilities, refineries, factories, consumer, commercial products and others. [5] Automotive painting operation is the main source of VOCs

emissions in the automotive manufacturing industry [6, 7]. VOCs emission from automotive painting consists of a mixture of high and low molecular weight organic compounds including aromatic hydrocarbons, esters, ketones, alcohols, and glycol ethers [7, 6]. It was reported that that 6.58 kg of VOCs is used as paint solvents per vehicle in a typical automotive plant in North America [7].

VOCs are of a concern because of their health and environmental impacts. Some VOCs degrade in the troposphere to produce different secondary pollutants that may be harmful to human health as well as to the environment [8, 9]. Some others are known to be carcinogenic or react in the atmosphere to form mutagenic or carcinogenic species [10]. Prolonged exposure to some VOCs could result in damage to liver and central nervous system [7, 11, 12]. VOCs also plays a major role in the formation of photochemical smog and various toxic by-products under sunlight [13 14] which in turn leads to respiratory effects in humans, visibility problems and cause damage to building materials and vegetation. For these reasons, environmental legislation requires elimination or control of large portion of VOC emission produced during different industrial activities [15] and this requires improved and efficient abatement methods, particularly for the treatment of dilute VOC-laden air streams [15].

Technologies generally considered in end of pipe control of VOCs emission include incineration, absorption, adsorption, catalytic and thermal oxidation, condensation, biofiltration and membrane separation [11, 16, 17, 18, 19, 20, 21]. Adsorption is a widely used method for VOC control because of its low cost and high capturing efficiency even at very low concentrations compared to other

VOCs control methods [6, 13,22, 23]. In addition, adsorption is a non-destructive control method allowing for the recovery of VOCs for possible recycle and reuse. Fixed-bed adsorption is one of the most widely used industrial and small scale air pollution control processes. Fixed bed adsorbers could be used to treat VOC-containing air streams over a wide range of flow rate, (several hundreds to hundreds thousands of cubic feet per minute) and VOCs concentrations (as low as several parts per billion by volume (ppbv)) [24, 25]. Hence, optimizing the design and operation conditions of the fixed-bed adsorber is evidently important to improve the efficiency and reduce the cost of VOC control.

The basis for traditional design and optimization approach of adsorption systems is the experimental data obtained with pilot scale systems. This approach could rarely be used to predict the response of the unit to variables other than those specifically tested for in a pilot scale system and it is also difficult to extrapolate the design to other applications [26]. Therefore, pilot plant design is usually expensive and time consuming. However, validated mathematical model can be used to facilitate the design and optimization of the adsorber by reducing the number of pilot scale testes required to evaluate various operation conditions which also reduces the related time and costs [27]. Once validated, mathematical models can also be used to predict response or sensitivity of the adsorber to changes in variables that can`t be easily measured [26, 28]. Earlier studies [29, 30, 31, 32, 33] that modeled VOC adsorption in a fixed bed adsorber focused on axial variation of adsorption and flow parameters. However, such a one-dimensional approach for simulating a fixed bed can have limited accuracy of prediction. Comparison of

results from experiments and one dimensional model of fixed bed adsorbers indicates the need for at least a two dimensional (radial and axial) model to simulate transport phenomena in a fixed bed adsorber [34]. The concentration wave fronts at the center and periphery of a fixed bed differ significantly when the ratio of column diameter to particle size is less or equal to 30 [34,35, 36]. It was also suggested that the channeling effect is significant even for a larger ratio of column diameter to the particle size [34, 37, 38]. Therefore, one-dimensional models are not sufficient to accurately describe transport phenomena in a fixed bed adsorber and a two dimensional (2D) model is needed [39, 40, 41].

Previous studies on modelling of dynamic adsorption of competing adsorbates focused on binary [42, 43 44] or ternary [45, 46] mixtures. However, most industrial emissions usually consist of mixture of more than three adsorbates, as is the case of emission from automotive painting booths [7, 47]. Hence, there is a need for developing a mathematical model that can accurately predict competitive adsorption of mixtures of large number of adsorbates. A comprehensive model for the study of adsorption process consists of the model for the analysis of dynamic adsorption (a macroscopic mass, energy and momentum conservation equations) and the equilibrium adsorption (isotherm equations). These two sets of models should be coupled and solved together.

1.2 Research Objectives

The goal of this research is to develop and validate a fully predictive two-dimensional mathematical model to study the process of adsorption of VOCs,

commonly emitted from automotive painting operations onto a fixed bed of beaded activated carbon (BAC). Hence, the following objectives can be described.

- Modeling and validation of the adsorption of single component VOC streams which will be done by (a) developing a fully predictive 2D mathematical model to solve the transport phenomena in a fixed bed adsorber during adsorption of VOC and validating the model with experimentally measured data for adsorption of various VOCs selected based on their molecular weight and or boiling point; and (b) performing sensitivity analysis to study the model response to changes in the adsorber's operation parameters and adsorbent properties.
- Modeling and validation of competitive adsorption of mixture of VOCs onto BAC which will be done by developing (a) a multicomponent competitive adsorption isotherm model that can predict equilibrium adsorption of n-component VOCs mixture using single-component isotherm parameters; (b) a fully predictive two-dimensional transient mathematical model for the transport of mass, energy and momentum during the competitive adsorption of n-component VOCs mixture onto a fixed bed of BAC.

These objectives will be achieved by modeling a small scale fixed-bed adsorber and conducting experiments using a similar set up and conditions to validate the model.

This research is significant for the study of VOCs adsorption because: (1) the model developed is fully predictive and could be used to significantly reduce the number of experiments needed and related costs for the design of new fixed bed adsorbers and optimization of the existing ones. (2) The model is sensitive to operation parameters and adsorbent property so it could be used for screening purpose during preliminary study and/ or to investigate the optimum operation condition. (3) The competitive adsorption model developed could be used to study adsorption of complex mixture of VOCs regardless of the number of components which is very important to enhance the understanding of competitive adsorption (4) The isotherm equation model developed can be used to predict the equilibrium capacity of the adsorbent for each component of the mixture during competitive adsorption using single component isotherm parameters alone. Overall this research is very important to increase our understanding of adsorption process in a fixed bed of porous adsorbent.

1.3 Thesis Outline

The thesis consists of four chapters, each of which will contribute to the main goal of the study. The second chapter focuses on the modelling and validation of adsorption of single component adsorbates from gaseous stream. Chapter 3 presents details on the modelling and validation of competitive adsorption of a mixture of VOCs. The second and the third chapters also review previous researches conducted in the area of study. Chapter 4 presents the conclusions and the implication of the results to the field of VOC control.

1.4 References

1. USEPA Definition of Volatile Organic Compounds (VOC), last upadated, 2009. http://www.epa.gov/ttn/naaqs/ozone/ozonetech/def_voc.htm (accessed 20/08/2013),
2. Directive 2004/42/CE of the European Parliament and the Council, 2004. http://eur-lex.europa.eu/LexUriServ/LexUriServ.do?uri=OJ:L:2004:143:0087:0096:EN:PDF (accessed 20/08/2013),
3. Berenjian, A.; Chan, N.; Malmiri, H. J., Volatile Organic Compounds removal methods: A review. *American Journal of Biochemistry and Biotechnology* **2012,** *8*, (4), 220-229.
4. Guenther, A., A global model of natural volatile organic compound emissions. *Journal of Geophysical Research* **1995,** *100*, (D5), 8873-8892.
5. Piccot, S. D.; Watson, J. J.; Jones, J. W., A global inventory of volatile organic compound emissions from anthropogenic sources. *Journal of Geophysical Research* **1992,** *97*, (D9), 9897-9912.
6. Golovoy, A.; Braslaw, J., Adsorption of automotive paint solvent on activated carbon. I. Equilibrium adsorption of single vapors. *Journal of the Air Pollution Control Association* **1981,** *31*, (8), 861-865.
7. Kim, B. R., VOC emissions from automotive painting and their control: A review. *Environmental Engineering Research* **2011,** *16*, (1), 1-9.
8. Wayne, R. P., *Chemistry of Atmospheres*. Clarendon: Oxford, 1991.
9. Finaly-Pitts, B. J., Pitts, J.N, *Atmospheric Chemistry: Fundamentals and Experimental Techniques* Wiley: New York, 1986.
10. Strauss, W., Mainwarning, S. J., *Air Pollution*. Edward Arnold: London, 1984.
11. Johnsen, D. L.; Mallouk, K. E.; Rood, M. J., Control of electrothermal heating during regeneration of activated carbon fiber cloth. *Environmental Science and Technology* **2011,** *45*, (2), 738-743.
12. Alcañiz-Monge, J.; Pérez-Cadenas, M.; Marco-Lozar, J., Removal of harmful volatile organic compounds on activated carbon fibres prepared by steam or carbon dioxide activation. *Adsorption Science and Technology* **2012,** *30*, (6), 473-482.
13. Das, D.; Gaur, V.; Verma, N., Removal of volatile organic compound by activated carbon fiber. *Carbon* **2004,** *42*, (14), 2949-2962.
14. Nevers, N.D, *Air Pollution Control Engineering*. Mc-Graw-Hill: Singapore, 2000.
15. Mota, J.P., Lyubchik, S. (eds), *Recent Advances in Adsorption Processes for Environmental Protection and Security*. Springer: The Netherlands, 2008.
16. Parmar, G. R.; Rao, N. N., Emerging control technologies for volatile organic compounds. *Critical Reviews in Environmental Science and Technology* **2009,** *39*, (1), 41-78.
17. Leethochawalit, M.; Bustard, M. T.; Wright, P. C.; Meeyoo, V., Novel vapor-phase biofiltration and catalytic combustion of volatile organic

compounds. *Industrial and Engineering Chemistry Research* **2001,** *40*, (23), 5334-5341.
18. Li, C.; Moe, W. M., Activated carbon load equalization of discontinuously generated acetone and toluene mixtures treated by biofiltration. *Environmental Science and Technology* **2005,** *39*, (7), 2349-2356.
19. Kim, K. J.; Kang, C. S.; You, Y. J.; Chung, M. C.; Seung, W. J.; Jeong, W. J.; Woo, M. W.; Ahn, H. G., Adsorption-desorption characteristics of modified activated carbons for volatile organic compounds 2006; Vol. 159, pp 457-460.
20. Kim, K. J.; Kang, C. S.; You, Y. J.; Chung, M. C.; Woo, M. W.; Jeong, W. J.; Park, N. C.; Ahn, H. G., Adsorption-desorption characteristics of VOCs over impregnated activated carbons. *Catalysis Today* **2006,** *111*, (3-4), 223-228.
21. Hashisho, Z.; Emamipour, H.; Cevallos, D.; Rood, M. J.; Hay, K. J.; Kim, B. J., Rapid response concentration-controlled desorption of activated carbon to dampen concentration fluctuations. *Environmental Science and Technology* **2007,** *41*, (5), 1753-1758.
22. Ramos, M. E.; Bonelli, P. R.; Cukierman, A. L.; Ribeiro Carrott, M. M. L.; Carrott, P. J. M., Adsorption of volatile organic compounds onto activated carbon cloths derived from a novel regenerated cellulosic precursor. *Journal of Hazardous Materials* **2010,** *177*, (1-3), 175-182.
23. Shonnard, D. R.; Hiew, D. S., Comparative environmental assessment of VOC recovery and recycle design alternatives for a gaseous waste stream. *Environmental Science and Technology* **2000,** *34*, (24), 5222-5228.
24. Calvert, S. A. E., Harold M. (eds.), *Handbook of Air Pollution Control Technology,*. John Wiley & Sons: New York, 1984.
25. *Handbook of Chemistry and Physics*. 54th Edition ed.; The Chemical Rubber Company: Cleveland.
26. Weber, W. J.; Smith, E. H., Simulation and design models for adsorption processes. *Environmental Science & Technology* **1987,** *21*, (11), 1040-1050.
27. Thomas, W. J.; Crittenden, B. D., *Adsorption technology and design*. Butterworth-Heinemann: Oxford Boston Johannesburg, 1998.
28. Xu, Z.; Cai, J. G.; Pan, B. C., Mathematically modeling fixed-bed adsorption in aqueous systems. *Journal of Zhejiang University: Science A* **2013,** *14*, (3), 155-176.
29. Fournel, L.; Mocho, P.; Brown, R.; Le Cloirec, P., Modeling breakthrough curves of volatile organic compounds on activated carbon fibers. *Adsorption* **2010,** *16*, (3), 147-153.
30. Joly, A.; Perrard, A., Linear driving force models for dynamic adsorption of volatile organic compound traces by porous adsorbent beds. *Mathematics and Computers in Simulation* **2009,** *79*, (12), 3492-3499.
31. Murillo, R.; García, T.; Aylón, E.; Callén, M. S.; Navarro, M. V.; López, J. M.; Mastral, A. M., Adsorption of phenanthrene on activated carbons: Breakthrough curve modeling. *Carbon* **2004,** *42*, (10), 2009-2017.
32. Puértolas, B.; López, M. R.; Navarro, M. V.; López, J. M.; Murillo, R.; García, T.; Mastral, A. M., Modelling the breakthrough curves obtained

from the adsorption of propene onto microporous inorganic solids. *Adsorption Science and Technology* **2010,** *28*, (8-9), 761-775.
33. Chuang, C. L.; Chiang, P. C.; Chang, E. E., Modeling VOCs adsorption onto activated carbon. *Chemosphere* **2003,** *53*, (1), 17-27.
34. Mohamadinejad, H.; Knox, J. C.; Smith, J. E., Experimental and Numerical Investigation of Two-Dimensional CO2 Adsorption/Desorption in Packed Sorption Beds Under Non-ideal Flows. *Separation Science and Technology* **2003,** *38*, (16), 3875-3904.
35. Cohen, Y.; Metzner, A. B., Wall effects in laminar flow of fluids through packed beds. *AIChE Journal* **1981,** *27*, (5), 705-715.
36. Yin, F.; Wang, Z.; Afacan, A.; Nandakumar, K.; Chuang, K. T., Experimental studies of liquid flow maldistribution in a random packed column. *Canadian Journal of Chemical Engineering* **2000,** *78*, (3), 449-457.
37. Cohen, Y.; Metzner, A. B., Wall effects in laminar flow of fluids through packed beds. *AIChE Journal* **1981,** *27*, (4), 705-715.
38. Cohen, Y.; Metzner, A. B., Wall effects in laminar flow of fluids through packed beds. *AIChE J.* **1981,** *27*, (4),.705-715.).
39. Benenati, R. F.; Brosilow, C. B., Void fraction distribution in beds of spheres. *AIChE Journal* **1962,** *8*, (3), 359-361.
40. Vortmeyer, D.; Winter, R. P., Improvement in reactor analysis incorporating porosity and velocity profiles. *German Chemical Engineering* **1984,** *7*, (1), 19-25.
41. Schwartz, C. E.; Smith, J. M., Flow distribution in packed beds. *Industrial & Engineering Chemistry* **1953,** *45*, (6), 1209-1218.
42. Lillo-Ródenas, M. A.; Fletcher, A. J.; Thomas, K. M.; Cazorla-Amorós, D.; Linares-Solano, A., Competitive adsorption of a benzene-toluene mixture on activated carbons at low concentration. *Carbon* **2006,** *44*, (8), 1455-1463.
43. Ahmed, M. J.; Mohammed, A. H. A. K.; Kadhum, A. A. H., Modeling of breakthrough curves for adsorption of propane, n-butane, and Iso-butane mixture on 5A molecular sieve zeolite. *Transport in Porous Media* **2011,** *86*, (1), 215-228.
44. Gironi, F.; Piemonte, V., VOCs removal from dilute vapour streams by adsorption onto activated carbon. *Chemical Engineering Journal.* **2011,** *172*, (2–3), 671-677.
45. Lu, L.; Wang, Q.; Liu, Y., Adsorption and separation of ternary and quaternary mixtures of short linear alkanes in zeolites by molecular simulation. *Langmuir* **2003,** *19*, (25), 10617-10623.
46. To, P. C.; Mariñas, B. J.; Snoeyink, V. L.; Wun, J. N., Effect of pore-blocking background compounds on the kinetics of trace organic contaminant desorption from activated carbon. *Environmental Science and Technology* **2008,** *42*, (13), 4825-4830.
47. Wang, H.; Jahandar Lashaki, M.; Fayaz, M.; Hashisho, Z.; Philips, J. H.; Anderson, J. E.; Nichols, M., Adsorption and desorption of mixtures of organic vapors on beaded activated carbon. *Environmental Science and Technology* **2012,** *46*, (15), 8341-8350.

CHAPTER 2 TWO-DIMENSIONAL MODELING OF VOLATILE ORGANIC COMPOUNDS ADSORPTION ONTO BEADED ACTIVATED CARBON

A version of this chapter was accepted for publication in Environmental Science & Technology, http://pubs.acs.org/doi/abs/10.1021/es402369u. Reproduced with permission from Dereje Tamiru Tefera, Masoud Jahandar Lashaki, Mohammadreza Fayaz, Zaher Hashisho, John H. Philips, James E. Anderson, Mark Nichols. 2013

2.1 Introduction

Adsorption onto activated carbon has been widely used for controlling emissions of volatile organic compounds (VOCs) at low concentration because of its cost effectiveness, high capturing efficiency and regenerability of the adsorbent for reuse [1, 2]. The fixed bed is one of the most widely used reactor configuration both in small and large scale VOC adsorption units. Therefore, detailed knowledge of transport phenomena in such an adsorber is essential for its proper design, performance analysis and optimization. Earlier studies [3, 4, 5, 6, 7] that modeled fixed bed absorber dynamics in the gas-phase focused on axial variation of adsorption and flow parameters. However, there is still a need for models that can accurately predict the two dimensional variation of transport variables, particularly during adsorption from dilute gas streams. Experimental investigations have confirmed that conventional one-dimensional models are not sufficient to describe transport phenomena in a fixed bed adsorber due to the radial variation of flow dynamics in addition to the axial one [8, 9, 10]. The temperature, velocity, and concentration gradients in the radial direction are significant and need to be accounted for, particularly when the particle to bed diameter ratio is less than 30 [11, 12]. Daszkowski and Eingenberger [13] also showed that the radial heat transfer could be accurately modelled only if radial flow variation is taken into account. Measurements of radial velocity and concentration profiles showed significant difference between the center and periphery of the reactor [14,15,]. Measuring radial variation of flow parameters is difficult. Therefore, developing a mathematical model that can accurately predict the two dimensional variation of transport

phenomena during adsorption of VOCs, particularly from dilute gas streams, is useful for improved design and optimization of fixed bed absorbers.

Automotive painting booths are the main source of VOCs emission during vehicle manufacturing. These emissions, which are typically captured using adsorption, consist of organic compounds, which contain different functional groups, and have a range of boiling points, and adsorption and desorption properties [16, 17]. Hence it is useful to understand adsorption dynamics of VOCs and the effect of operation conditions on the adsorber performance. The main objective of this study is to develop a comprehensive model that can accurately simulate transport phenomena during VOC adsorption in a fixed bed adsorber. For this purpose, a two-dimensional model, solved using the finite element method, was developed and validated using measured data. The model was also used to examine the effect on the adsorber performance of variation of relevant operation conditions, such as adsorbate loading, carrier gas temperature, pressure drop, and adsorbent particle size.

2.2 Model Development and Validation

2.2.1 Physical Model and Assumptions

The simulated adsorber consisted of a reactor with a 0.76 cm inner radius (R) containing a 12 cm long fixed-bed of BAC with 0.75 mm mean particle diameter (d_p)**.** A 10 standard liters per minute (SLPM) air stream containing 1000 ppmv of the VOC entered from the top of **t**he reactor at a superficial velocity (Vs) of 0.914 m/s and exited from the bottom of the reactor. Major assumptions used in model

development include negligible variation of flow properties in the angular direction, negligible adsorption of the carrier gas, ideal gas behavior, and symmetric flow condition and geometry along the adsorber center plane.

2.3 Governing Transport Phenomena

2.3.1 Adsorbate Mass Balance

Derivation of the governing equation for the mass transport is based on the concept that the fixed bed of porous adsorbent particles consists of a stationery (solid adsorbent) phase and a mobile (gas) phase. The adsorbate is transported in the mobile phase by convection and dispersion. The advection-dispersion transport equation is derived based on the conservation of adsorbate mass flux entering and leaving a small representative element of the bed (equation 2.1). Definition and value of the model input parameters and variables are presented in Table 2.2.

$$\boldsymbol{\varepsilon_r \frac{\partial C}{\partial t} - \nabla(D\varepsilon_r \nabla c) + \nabla(uc) + S_m = 0} \quad \text{.....2.1}$$

The bed porosity, $\boldsymbol{\varepsilon_r}$, varies with radial distance from the reactor center (equations 2.2, 2.3, and 2.4) [18]

$$\boldsymbol{\varepsilon_r = \varepsilon_b \left(1 + f * \exp\left(6 \frac{R-r}{d_p}\right)\right)} \quad \text{.....2.2}$$

where $\boldsymbol{\varepsilon_b = 0.379 + \frac{0.078}{\left(\frac{D_b}{d_p}\right)^{-1.8}}}$ 2.3

$$f = \boldsymbol{\frac{1-\varepsilon_b}{\varepsilon_b}} \quad \text{.....2.4}$$

$$\text{and } D = \begin{vmatrix} D_r & 0 \\ 0 & D_{ax} \end{vmatrix} \quad \text{.....2.5}$$

where the radial and axial mass dispersion coefficients [19, 14] are given by equations 2.6a and 2.6b, respectively.

$$\mathbf{D_r} = \left(\boldsymbol{\alpha_0} + \frac{\mathbf{ScRe_p}}{\mathbf{8}}\right)\frac{\mathbf{D_{AB}}}{\boldsymbol{\varepsilon_b}} \quad \text{.....2.6a}$$

$$\mathbf{D_{ax}} = \left(\boldsymbol{\alpha_0} + \frac{\mathbf{ScRe_p}}{\mathbf{2}}\right)\frac{\mathbf{D_{AB}}}{\boldsymbol{\varepsilon_b}} \quad \text{.....2.6b}$$

The governing transport equation in the solid phase (adsorbent) is similar to that in the gas phase except that the contribution of convection and dispersion to the adsorbate transport is negligible and the main mass transport takes place by diffusion of the adsorbate in the porous adsorbent particles. Such diffusive transport takes place by pore and /or surface diffusion which can be modelled at individual particle level, but is time and computationally intensive. Alternatively, an approximation using the linear driving force (LDF) [20] model can be used (equation 2.7) to describe the diffusion of the adsorbate in the adsorbent. The LDF has similar accuracy to more complex diffusion models in predicting mass transfer in the adsorbent particle [20-29]. Coupling of the solid and gas phase governing equations is made through source/sink terms, whereby the mass sink in the gas phase is equal to the mass source in the solid phase.

$$\frac{\partial \mathbf{C_s}}{\partial \mathbf{t}} = \mathbf{S_m} \quad \text{.....2.7}$$

S_m is proportional to the adsorbed phase concentration gradient and mass transfer will take place until equilibrium is reached (equation 2.8).

$$\mathbf{S_m} = \mathbf{k_{ov}}(\mathbf{c_{se}} - \mathbf{c_s}) \quad \text{.....2.8}$$

$$\mathbf{c_{se}} = \boldsymbol{\rho_p}\mathbf{q_e} \quad \text{.....2.9}$$

The overall mass transfer coefficient, K_{ov}, accounts for the external (gas-solid interface) diffusion, pore diffusion and surface diffusion mass transfer resistances[19]:

$$\mathbf{k_{ov}} = \frac{\mathbf{60\varepsilon_p C_o D_{eff}}}{\tau_p \mathbf{C_{so} d_p}^2} \quad \text{2.10}$$

$$\boldsymbol{\varepsilon_p} = \mathbf{V_{pore}}\boldsymbol{\rho_p} \quad \text{2.11}$$

$$\boldsymbol{\rho_p} = \frac{\boldsymbol{\rho_b}}{\mathbf{1}-\boldsymbol{\varepsilon_b}} \quad \text{2.12}$$

$$\boldsymbol{\tau_p} = \frac{\mathbf{1}}{\boldsymbol{\varepsilon_p}^2} \quad \text{2.13}$$

The effective diffusion coefficient is the resultant of molecular and Knudsen diffusion coefficients:

$$\frac{\mathbf{1}}{\mathbf{D_{eff}}} = \frac{\mathbf{1}}{\mathbf{D_{AB}}} + \frac{\mathbf{1}}{\mathbf{D_k}} \quad \text{2.14}$$

where D_{AB} [30] and D_k [31] are expressed as:

$$\mathbf{D_{AB}} = \mathbf{10^{-3} T^{1.75}} \frac{\sqrt{\frac{\mathbf{M_A+M_B}}{\mathbf{M_A M_B}}}}{\mathbf{P}\left((\sum \mathbf{v})_\mathbf{A}^{\mathbf{0.33}} - (\sum \mathbf{v})_\mathbf{B}^{\mathbf{0.33}}\right)^2} \quad \text{2.15}$$

$$\mathbf{D_k} = \mathbf{9700 r_p}\sqrt{\frac{\mathbf{T}}{\mathbf{M_A}}} \quad \text{2.16}$$

A temperature-dependent Langmuir isotherm (equation 2.17) was used to model the equilibrium condition because of its accuracy at low concentration [32].

$$\mathbf{q_e} = \frac{\mathbf{q_m b\ c}}{\mathbf{1+bc}} \quad \text{2.17}$$

$$\mathbf{b} = \mathbf{b_o exp}\left(\frac{-\Delta \mathbf{H_{ad}}}{\mathbf{R_g T}}\right) \quad \text{2.18}$$

2.3.2 Energy Balance

In balancing the energy fluxes from and into a small representative element of the bed, two basic assumptions were made, namely thermal homogeneity between the solid and gas phases and negligible viscous heat dissipation. Heat transport takes place by convection and diffusion (equation 2.19), similar to mass transport.

$$\mathbf{C_v}\frac{\partial \mathbf{T}}{\partial \mathbf{t}} + \mathbf{C_{pf}}\boldsymbol{\rho_f}\mathbf{u}.\nabla\mathbf{T} - \nabla.(\mathbf{k_{ef}}\nabla\mathbf{T}) = \mathbf{S_h} \quad \text{2.19}$$

The effective heat capacity of the solid and gas phases, $\mathbf{C_v}$, is calculated using equation 2.20.

$$\mathbf{C_v} = (1-\boldsymbol{\varepsilon_b})\boldsymbol{\rho_p}\mathbf{C_{pp}} + \boldsymbol{\varepsilon_b}\boldsymbol{\rho_f}\mathbf{C_{pf}} \quad \text{2.20}$$

K_{ef} is the symmetric thermal diffusion tensor:

$$\mathbf{K_{ef}} = \begin{vmatrix} \mathbf{K_r} & \mathbf{0} \\ \mathbf{0} & \mathbf{K_{ax}} \end{vmatrix} \quad \text{2.21}$$

The axial and radial thermal dispersion coefficients (K_{ax} and K_r) account for the stagnant bed conductivity, K_b, and the effect of convection on the thermal conductivity (the second term in equations 2.22a and 2.22b)[18].

$$K_r = \mathbf{K_b} + \frac{\mathbf{1}}{\mathbf{8}}\mathbf{Pe_o}\mathbf{k_f}. \quad \text{2.22a}$$

$$K_{ax} = \mathbf{K_b} + \frac{\mathbf{1}}{\mathbf{2}}\mathbf{Pe_o}\mathbf{k_f} \quad \text{2.22b}$$

$$K_b = (\mathbf{1} - \boldsymbol{\varepsilon_b})\mathbf{k_p} + \boldsymbol{\varepsilon_b}\mathbf{k_f} \quad \text{2.23}$$

Because other sources such as viscous dissipation are considered negligible, the main heat source to the system during adsorption is the heat of adsorption (equation 2.24):

$$\mathbf{S_h} = (-\Delta\mathbf{H_{ad}})\frac{\mathbf{dc_s}}{\mathbf{dt}} \quad \text{2.24}$$

The heat of adsorption is dependent on the properties of the adsorbate and adsorbent [33]:

$$\Delta H_{ad} = 103.2 + 1.16\alpha + 0.76\Delta H_{vap} - 3.87IP - 0.7\gamma - 26.1w_{mic} \quad \text{..... 2.25}$$

2.3.3 Momentum Balance

The gas is assumed Newtonian and its flow behavior in porous media depends on properties of the solid matrix and the flowing gas and the flow velocity. The porous matrix is stationery and its linear momentum is negligible hence the most significant interaction forces contributing to momentum dissipation are the friction forces that the gas encounters at the boundaries of the pore. In this study, a modified momentum balance equation (equation 2.26) which accounts for Darcy and Brinkman viscous terms, Forchheimer inertial term, and Navier–Stokes' convective term [18] was used to model the non-Darcy gas flow in the BAC.

$$\frac{\rho_f}{\varepsilon_r}\left(\left(\frac{\partial u}{\partial t}\right) + (u.\nabla)\frac{u}{\varepsilon_r}\right) = -\nabla P + \nabla.J - S + F \quad \text{..... 2.26}$$

where the shear stress is defined in terms of gas viscosity (equation 2.27).

$$J = \left(\frac{1}{\varepsilon_r}\left(\mu_f \nabla u + (\nabla u)^T - \frac{2}{3}\mu_f(\nabla.u)I\right)\right) \quad \text{..... 2.27}$$

The momentum sink of the flow in a fixed bed of porous adsorbent is accounted for by Darcy's friction loss, Forchheimer's inertial term, and an adsorption sink:

$$S = \left(\frac{\mu_f}{K} + \beta|v| + \frac{S_m}{\varepsilon_r}\right)u \quad \text{..... 2.28}$$

The continuity equation accounts for the compressibility of the gas and an adsorption sink:

$$\frac{\partial(\varepsilon_r \rho_f)}{\partial t} + \nabla.(\boldsymbol{\rho_f \mathbf{u}}) = S_m \quad \text{2.29}$$

The bed permeability (K) is a function of particle diameter and bed porosity [18]

$$K = \frac{\varepsilon_b^3 d_p^2}{150(1-\varepsilon_b)^2} \quad \text{2.30}$$

Forchheimer's drag coefficient (β) is a function of bed permeability and particle and bed diameter [18]:

$$\boldsymbol{\beta = \rho_f \frac{C_F}{\sqrt{K}}} \quad \text{2.31}$$

$$C_F = 0.55\left(1 - 5.5\left(\frac{d_p}{D_b}\right)\right) \quad \text{2.32}$$

2.3.4 Initial/ Boundary Conditions and Input Parameters

For mass transfer, a concentration boundary condition (BC) at the inlet and a flux boundary condition at the outlet were used. For heat transfer, a temperature boundary condition at the inlet, a constant flux (outflow) boundary condition at the outlet, and a convective heat flux at the wall were specified. For momentum balance, a normal velocity boundary condition at the inlet and an atmospheric pressure were specified at the outlet Table 2.1.

Table 2.1.Initial/ Boundary conditions and input parameters

Physics	Inlet (Z=H)	Outlet (Z=0)	Adsorber wall (r=R)	Initial condition (t=0)
Mass transfer	$c=c_o$ $c_s=c_{so}$	Boundary flux $-n.(D\nabla c)=0$ $-n.(D\nabla c_s)=0$	Zero flux	$c=0$ $c_s=0$
Heat transfer	$T=T_{inlet}$	$-n.(K\nabla T)=0$	$q_o = k_w(T_w - T)$	T=295K
Momentum transfer	V_s=0.914 m/s	P=1 atm	No slip	P=1 atm u=0

Parameters used in the current simulation and their respective sources are provided in Table 2.2.

Table 2.2. Model parameters

Parameter	Description	Value /equation	Units	Source
b	Temperature-dependent Langmuir affinity coefficient		m^3/kg	[32]
$\mathbf{b_o}$	Pre-exponential constant in Langmuir isotherm	Table 2.2	m^3/kg	
c	Gas phase concentration		kg/m^3	Equation 2.1
$\mathbf{C_F}$	Empirical correction factor for Forchheimer's drag coefficient calculation		1	Equation 2.32
$\mathbf{c_o}$	Inlet gas concentration	1000	ppmv	Table 2.1
c_s	Adsorbed phase concentration		kg/m^3	Equation 2.7
c_{se}	Equilibrium adsorbed phase concentration		kg/m^3	Equation 2.9
c_{so}	Adsorbed phase concentration equilibrium with inlet gas phase concentration.		kg/m^3	Equation 2.10
$\mathbf{C_{pf}}$	Gas heat capacity	$286.9\left(3.33 + 0.000575T^2 - \frac{1600}{T^2}\right)$	J/kg.K	[34]
$\mathbf{C_{pp}}$	Adsorbent particle heat capacity	706.7	J/kg.K	[35]
$\mathbf{C_v}$	Effective volumetric heat capacity of the solid-gas system		$J/(m^3.K)$	Equation 2.20
D	Symmetric mass dispersion tensor		cm^2/s	Equation 2.5
$\mathbf{D_{AB}}$	Molecular diffusivity of the adsorbate in air		cm^2/s	Equation 2.15
D_{ax}	Axial dispersion coefficient		cm^2/s	Equation 2.6b

$\mathbf{D_b}$	Reactor diameter	0.01524	m	Measured
D_{eff}	Effective diffusion coefficient		cm^2/s	Equation 2.14
D_k	Knudsen diffusivity		cm^2/s	Equation 2.16
d_p	Average particle diameter	0.00075	m	[17]
D_r	Radial dispersion coefficient		m^2/s	Equation 2.6a
F	Body force		N/m^3	Equation 2.26
$\mathbf{\Delta H_{ad}}$	Heat of adsorption		kJ/mol	Equation 2.25
$\mathbf{\Delta H_{vap}}$	Adsorbate heat of vaporization		kJ/mol	[33-35]
J	Shear stress		N/m^2	Equation 2.27
K	Bed permeability		m^2	Equation 2.30
$\mathbf{k_{ax}}$	Axial thermal diffusion coefficient		W/m.K	Equation 2.22b
$\mathbf{k_b}$	Stagnant bed thermal conductivity		W/m.K	Equation 2.23
k_{ef}	Symmetric thermal diffusion coefficient		W/m.K	Equation 2.21
k_f	Air thermal conductivity	$1.521 \times 10^{-11}T^3 - 4.8574 \times 10^{-8}T^2 + 1.084 \times 10^{-4}T - 0.00039333$	W/m.K	[36]
$\mathbf{k_{ov}}$	Overall mass transfer coefficient			Equation 2.10
$\mathbf{k_p}$	Adsorbent particle thermal conductivity	0.17	W/m.K	[37]
$\mathbf{k_r}$	Radial thermal diffusion coefficient		W/m.K	Equation 2.22a
$\mathbf{k_w}$	Wall heat transfer coefficient	$\frac{2.4}{d_p}K_{bed}+0.054\frac{K_f}{d_p}\left(1-\frac{d_p}{D_b}\right)Re_p P_r^{1/3}$	1	[38]

IP	Ionization potential		eV	[33]
M_A and M_B	Molecular weight of adsorbate and air, respectively		g/mol	
N	Number of data points			
P	Pressure		Pa	Equation 2.26
$\mathbf{Pe_o}$	Molecular Peclet number for heat transfer	$\frac{V_s \rho_f C_{pf} d_p}{K_f}$	1	[39]
$\mathbf{p_r}$	Prandtl number	$\frac{\mu_f C_{pf}}{k_f}$	1	[38]
q_e	Adsorbent equilibrium capacity		g/g	Equation 2.17
q_m	Adsorbent maximum equilibrium capacity		g/g	Table 2.3
r	Variable radial distance		m	
R	Radius of the adsorber	$D_b/2$	m	
Re_p	Particle Reynolds number	$\frac{\rho_f V_s d_p}{\mu_f}$	1	[19]
R_g	Ideal gas constant	8.314	J/(mol.K)	
S	Momentum sink		N/ m^3	
Sc	Schmidt number	$\frac{\mu_f}{\rho_f D_{AB}}$	1	[19]
$\mathbf{S_h}$	Heat source		J/(m^3.s)	Equation 2.24
$\mathbf{S_m}$	Mass sink		kg/(m^3.s)	Equation 2.1
t	Adsorption time		s	Equation 2.1
T	Temperature		K	Equation 2.19
T_{inlet}	Gas inlet temperature	300	K	BC1
$\mathbf{T_w}$	Wall temperature	295	K	BC1
u	Gas flow velocity vector		m/s	Equation 2.26

$\|\mathbf{v}\|$	Resultant velocity		m/s	Equation 2.28
$\mathbf{V_{pore}}$	Adsorbent pore volume	0.57	cc/g	Measured
$\mathbf{V_s}$	Superficial velocity	$\frac{4Q}{\pi(D_b)^2}$	m/s	Calculated
$\mathbf{w_{mic}}$	Average micropore width	1.02	nm	Measured
Z	Axial distance		m	

Greek Symbols

Parameter	Description	Value /equation	Unit	Source
α	Polarizability		(cm^3x10^{-24})	[33]
$\boldsymbol{\alpha_0}$	Empirical correction factor for mass diffusion terms	20	1	[19]
$\boldsymbol{\beta}$	Forchheimer's drag coefficient		kg/m^4	Equation 2.31
γ	Surface tension		mN/m	[33]
$\boldsymbol{\varepsilon_b}$	Bulk bed porosity		1	Equation 2.3
$\boldsymbol{\varepsilon_p}$	Particle porosity		1	Equation 2.11
$\boldsymbol{\varepsilon_r}$	Bed porosity as a function of radial distance from the center			Equation 2.2
μ_f	Gas viscosity		Pa.s	COMSOL material database
$\boldsymbol{\rho_b}$	Bulk bed density	606	kg/m^3	Measured
$\boldsymbol{\rho_f}$	Gas density		kg/m^3	COMSOL material database
$\boldsymbol{\rho_p}$	Particle density		kg/m^3	Equation 2.12

τ_p	Particle tortuosity	1	Equation 2.13
$(\sum v)_A$ $(\sum v)_B$	Atomic diffusion volumes	1	[30]

2.3.5 Solution Method

Simulation of the coupled mass, energy and momentum balance and constitutive equations was performed using COMSOL Multiphysics version 4.3a where the developed governing equations were solved numerically using the finite element method.

COMSOL's built-in models for mass transfer in a porous adsorbent assume instantaneous equilibrium between the gas and the adsorbent and negligible mass transfer resistance, which is not the case for adsorption from dilute streams where the mass transfer resistance is significant. Hence, simulation of mass transfer was performed using equation-based modelling through COMSOL's PDE interface and coupled to the built-in energy and momentum transport models.

Best modeling practices suggest the use of higher order elements; at least second order element and even higher order element should be used for convective term to avoid solution instability [40-42]. In this study a second-order element for concentration, temperature and pressure and a third-order element for velocity field were used with systematic mesh refinement until a grid-independent solution was obtained, as confirmed by the calculated 0.42% relative error in concentration using 13,847 elements and 26,772 elements.

2.3.6 Experimental Method

To validate the model, breakthrough experiments were performed using four selected VOCs. A stainless steel tube with a 0.76 cm inner radius and a height of 15 cm was filled with 13.3 g of microporous BAC. The reactor was loaded in such a way that the net height of the BAC bed was 12 cm. A 1.5 cm thick glass wool layer was used at the top and bottom of the reactor to support the bed. The effect of the glass wool layer on the flow and adsorption was considered negligible. The BAC had a BET area of 1390 m^2/g, micropore volume of 0.51 cm^3/g, and total pore volume of 0.57 cm^3/g. The concentration at the outlet of the reactor was measured using a flame ionization detector (FID) (Baseline Mocon, Series 9000).

For the validation of the temperature profile a 0.9 mm thermocouple (Omega) was inserted at the center of the reactor to measure instantaneous temperatures during adsorption. The pressure drop across the adsorbent bed during adsorption was determined as the difference between the pressure drop across the reactor (measured with a mass flow controller, Alicat Scientific) with and without the BAC.

To determine the Langmuir model parameters, the adsorption isotherms for acetone, benzene, and toluene were determined gravimetrically using a sorption analyzer (TA Instruments, model VTI-SA) at 25°C and nitrogen as carrier gas. A detailed description of the experimental set-up was presented elsewhere[17]. The system logged the equilibrium weight of the BAC sample (3–5 mg) in response to a step change in the concentration of the adsorbate in the carrier gas. The

equilibrium was assumed to be reached when the weight change is less than 0.001 wt percent in 5 min. For 1, 2, 4-trimethybenzene, the isotherm was obtained by completing a mass balance on a reactor loaded with 7g of BAC and adsorbing at 250, 500 and 1000 ppmv of 1, 2, 4-trimethybenzene in a 10 SLPM air stream at 25^{o}C. The adsorption setup and method is similar to the one used in the model validation experiments.

The non-zero data points from the model and experiment were compared and evaluated using the mean relative absolute error (MRAE) [43].

$$\text{MRAE} = \frac{\mathbf{1}}{\boldsymbol{N}} \sum_{\mathbf{1}}^{\boldsymbol{N}} \left| \frac{|\boldsymbol{experimental\ value - modelled\ value}|}{\boldsymbol{experimental\ value}} * \mathbf{100} \right| \quad \text{.....2.34}$$

When calculating the MRAE between measured and modelled temperature, the temperature was expressed in °C to avoid apparent low relative error bias from expressing the temperature in K.

The overall error in predicting the concentration and temperature was also evaluated using the root mean square error (RMSE) normalised by the influent stream concentration (in ppmv) and temperature (in °C), respectively [44].

$$\text{RMSE} = \sqrt{\frac{\mathbf{1}}{\boldsymbol{N}} \sum_{\mathbf{1}}^{\boldsymbol{N}} \left(\frac{\boldsymbol{experimental\ value - modelled\ value}}{\boldsymbol{influent\ stream\ value}} \right)^{\mathbf{2}}} * \mathbf{100} \quad \text{.....2.35}$$

2.4 Results and discussion

2.4.1 Isotherm Parameters

The Langmuir isotherm parameters were determined by fitting measured experimental data for each adsorbate to the linearized isotherm equation (equation 2.36). In this equation the slope of the lines is $\left(\frac{1}{bq_m}\right)$ and the y-intercept is $\left(\frac{1}{q_m}\right)$ are determined graphically Figure 2.1.

$$\frac{1}{q_e} = \frac{1}{bq_mC} + \frac{1}{q_m} \quad \text{.....2.36}$$

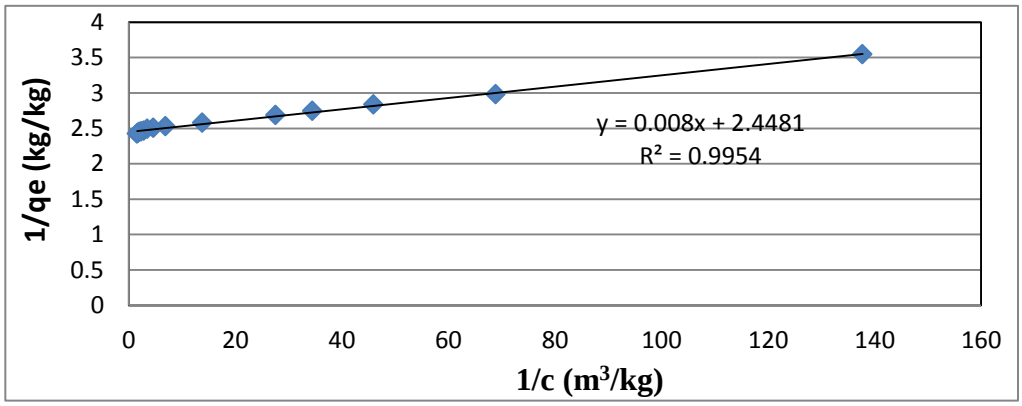

a

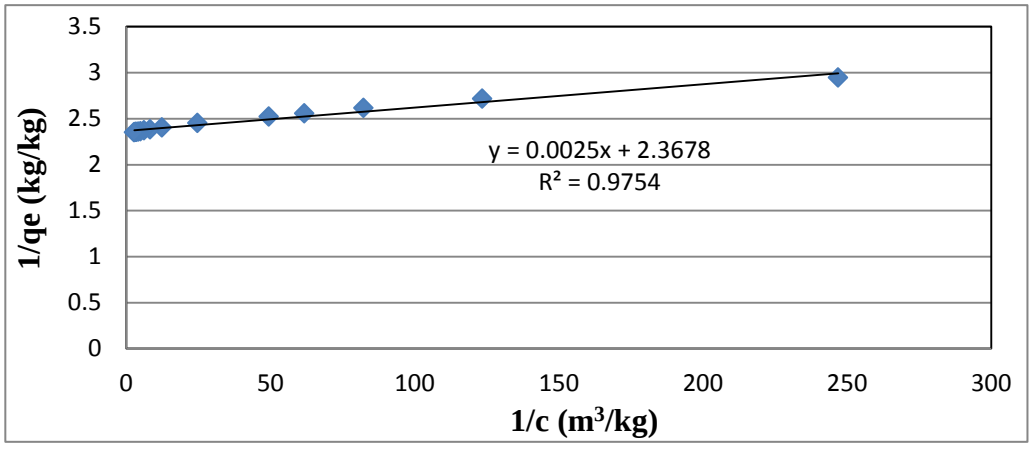

b

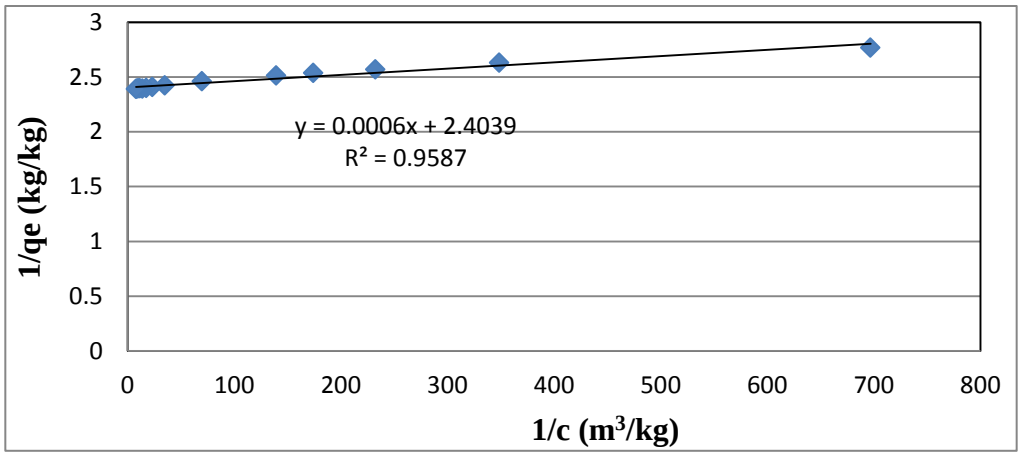

c

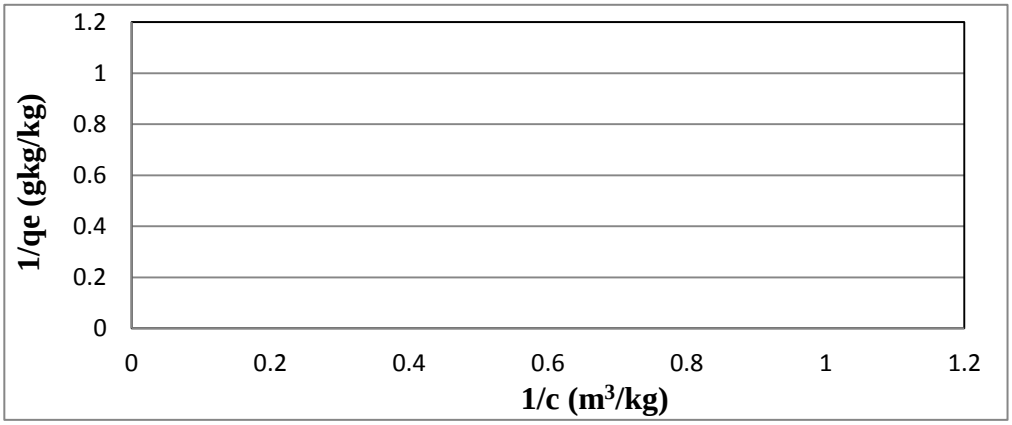

d

Figure 2.1. Linearized form of Langmuir isotherm to determine the isotherm parameters for (a) acetone, (b) benzene (c) toluene (d) 1, 2, 4-trimethybenzene (TMB)

The temperature dependent Langmuir affinity coefficient at 25^{o}C (b_{25}) was determined from the figures and used to determine the pre-exponential constant, b_o (Equation 36).

$$b_o = \frac{b_{25}}{exp\left(\frac{-\Delta H_{ad}}{TR}\right)} \quad \text{..... 2.37}$$

Table 2.3 describes summery of the Langmuir isotherm parameters.

Table 2.3 Langmuir isotherm parameters

Compounds	q_m (kg/kg)	b_{25} (m^3/kg)	b_o
Acetone	0.41	306	3.38E-07
Benzene	0.42	947	1.45E-07
Toluene	0.42	4006	1.38E-07
1, 2, 4-Trimethybenzene	0.46	7241	1.54E-11

2.4.2 Model Validation

Breakthrough experiments were used for validating the model performance because the concentration profile is coupled to the other flow variables such as flow velocity, pressure and temperature. Figure 2.2 shows modelled and measured breakthrough curves of individual organic adsorbates selected based on their range of boiling points, acetone (56^{o}C), benzene (80^{o}C), toluene (111^{o}C) and 1, 2, 4-trimethylbenzene (TMB) (170^{o}C). The model predicted the experimental breakthrough curves for the selected VOCs with an overall MRAE of 2.6% and RMSE of 1.0%. The agreement between the model and the experimental results is encouraging, as the model only uses independently determined properties of the adsorbent and adsorbate, and the adsorber geometry and operating conditions.

The model and experiments revealed a sharper breakthrough curve for acetone (Figure 2.2a) and a more gradual breakthrough curve for TMB (Figure 2.2d). This is because among the selected adsorbates, acetone is the smallest in size with the lowest diffusion resistance while TMB is the largest with the highest diffusion resistance. The good agreement supports the accuracy of the model assumptions, equations, and parameters. It also suggests that the model could be used to study the adsorption dynamics of a wide range of adsorbates, including the VOCs in

paint emissions which consists of a large number of organic compounds with a range of functional groups and physical properties [16].

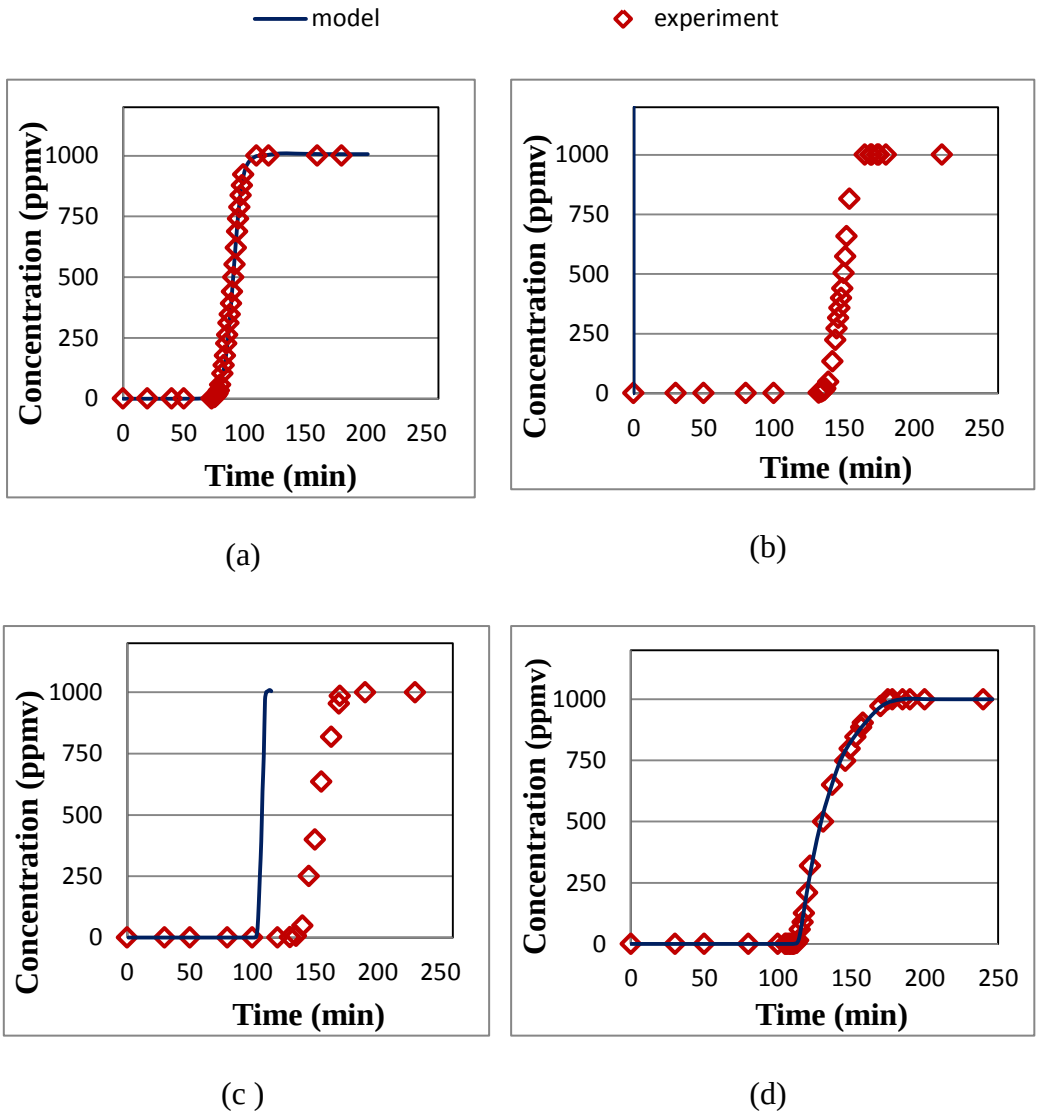

Figure 2.2. Comparison of the modeled and experimental breakthrough curves of acetone, (b) benzene, (c) toluene and (d) 1,2,4-trimethylbenzene on BAC. MRAE and RMSE were 2.0 and 1.2 % for acetone, 0.4 and 1.1 % for benzene, 4.0% and 1.0 % for toluene, and 4.0% and 0.7 % for TMB, respectively

2.4.3 Adsorbed Phase Concentration Distribution

Figure 2.3 shows the variation of axial and radial adsorbed-phase concentration for benzene. As the adsorbate is fed into the bed, the inlet portion of the bed becomes saturated and the mass transfer zone moves down the bed until the entire bed is saturated. The variation of the adsorbed phase concentration in the radial direction shows that the wall region of the bed is saturated earlier than the bed center because of channelling near the wall. This would be seen as an earlier breakthrough than if the model was a one-dimensional model along the bed center line.

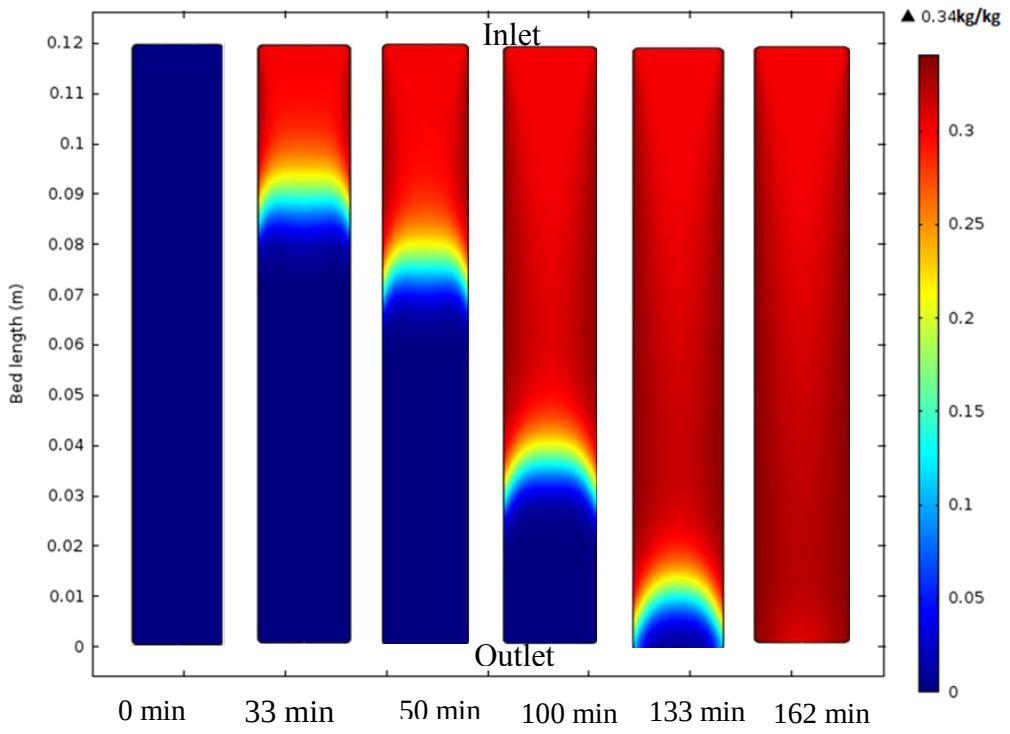

(a)

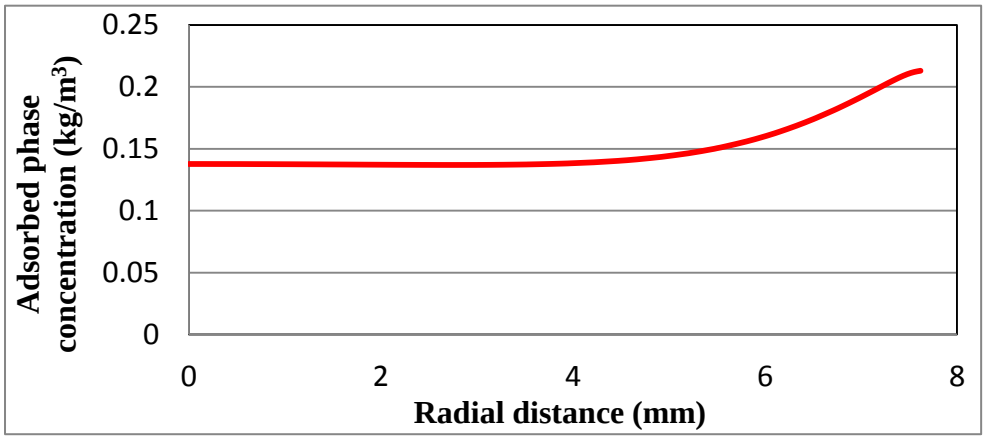

(b)

Figure 2.3. Solid-phase concentration of benzene on BAC indicating earlier saturation at the bed periphery compared to the bed center. (a) Progress in bed saturation with benzene over time and (b) the radial adsorbed phase concentration of benzene in the mass transfer zone (Z = 90 mm from the outlet, t= 33 min)

2.4.4 Temperature Distribution

The model results for two-dimensional temperature distribution during benzene adsorption reveal that the thermal wave advances through the bed with the mass transfer zone (MTZ) but at a higher velocity (Figure 2.3a). At t=33min, the MTZ is at 30 mm from the reactor inlet (Figure 2.3a) whereas the heat transfer zone is at about 40 mm (Figure 2.4a). Adsorption is an exothermic process and the bed temperature could increase depending on the adsorbate loading and heat of adsorption. The BAC bed temperature was highest for 1, 2, 4-trimethybenzene followed by toluene, benzene, and acetone (Figure 2.4b). This order is the same as the order of the heat of adsorption for the selected compounds. Figure 2.4 b reveals that the bed temperature during adsorption also varied across the bed, and is higher at the center than at the periphery due to the convective heat transfer at the wall. The results obtained using this model are consistent with previous experimental measurements [9, 39, 45, 46] which supports the reliability of this model to predict instantaneous radial and axial temperature profiles accurately for the VOCs evaluated. Similarly, the model predicted the transient temperature profile at the center of the bed (r=0.0 cm, z=8.0 cm, Figure 2.4c) with a MRAE of 0.8% and RMSE of 3.9%.

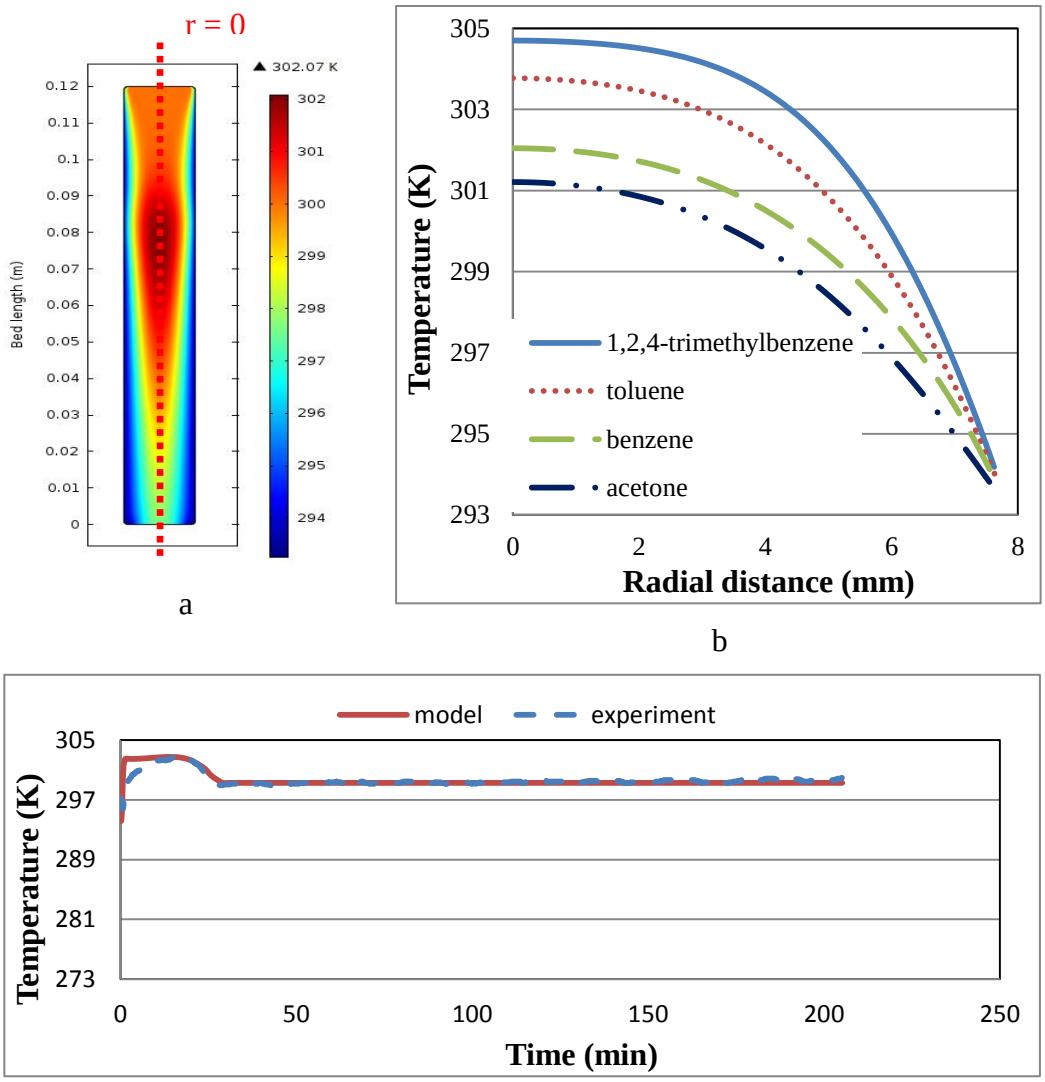

Figure 2.4.Temperature distribution during adsorption on BAC: (a) bed temperature profile 33 min after the start of benzene adsorption, (b) radial temperature profile during adsorption of acetone, benzene, toluene and 1,2,4-trimethylbenzene in the respective mass transfer zone and (c) comparison of modelled and measured temperature profile at the center of the reactor (r=0.0 cm, z= 8.0 cm)

2.4.5 Pressure Distribution and Velocity Field

Pressure drop is mainly influenced by the porosity of the adsorbent bed. The lowest pressure drop during benzene adsorption occurs at the outlet of the reactor and the maximum at the inlet (Figure 2.5). The modelled net pressure drop across the bed after 33min of adsorption is about 3.0 kPa which is comparable to the experimentally measured one (3.4 kPa). The MRAE (11.8 %) could be due to the use of gas viscosity instead of effective viscosity [47, 38] in the model and/or experimental error in measuring the pressure drop. The axial variation of pressure drop reflects axial variation of velocity (Figure 2.5). The axial flow velocity decreased sharply in the inlet region because the flow encounters high bed resistance and further reduction in the MTZ (40 mm from the inlet at 33min) due to the additional momentum sink during adsorption, and increased towards the outlet as the pressure drop linearly decreased and enabled the gas to expand (Figure 2.5). The higher pressure drop at the top of the reactor stabilizes the flow and allows sufficient contact time for mass transfer and reduce the effect of channeling (Figure 2.3a). This agrees with Chahbani and Tondeur's conclusion on the importance of pressure drop in fixed-bed adsorption[45].

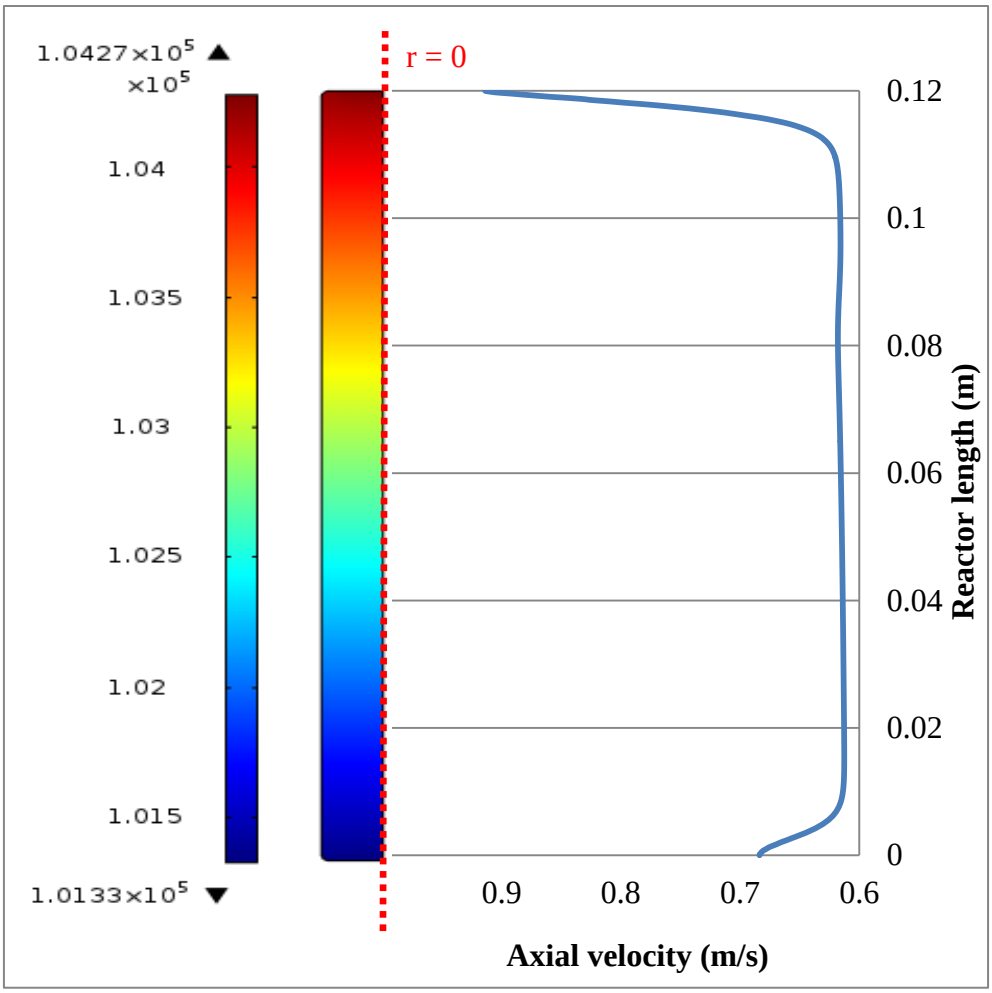

Figure 2.5. Variation of pressure and axial velocity in the bed during adsorption of benzene at 33 min after the start of adsorption

2.4.6 Parametric Study

In typical industrial applications, absorbers are often downstream of the plant and the absorber's performance could be affected by the performance and variation in process parameters of upstream plant operations. Therefore, it is useful to understand how the adsorber performance is affected when its operational parameters and input conditions are varied.

2.4.6.1 Effect of Adsorbate Loading, Carrier Gas Temperature, and Superficial Velocity

The effect of carrier gas temperature on adsorption of benzene was modelled and experimentally validated. Increasing the inlet gas temperature from 300K to 308K resulted in 22.5% reduction in the bed service time (defined as the time when the outlet adsorbate concentration is 1% of the inlet, i.e. the 1% breakthrough time) because higher temperature lowers the adsorption capacity of the adsorbent (Figure 2.6a). Good agreement was observed between the model and experimental results.

To investigate the effect of adsorbate inlet concentration on the bed temperature, benzene concentration in the inlet air was incrementally increased from 1,000 ppmv to 30,000 ppmv in the model. The maximum adsorption temperature attained for each case is plotted against the inlet concentration in Figure 2.6b. The increase in the adsorbent temperature is directly proportional to benzene concentration because of the proportionately higher heat released per unit of gas flow through the adsorber. This result is consistent with earlier experimental measurements[48].

To investigate the effect of the superficial velocity, every other conditions and parameters were kept constant and the base case superficial velocity was increased and decreased by a factor of two. The 5% breakthrough time decreased by (55%) for 2Vs while it increased by 109% for Vs/2 (Figure 2.6c). A slight change in the shape of the breakthrough curve was also observed as indicated by the throughput ration (TPR) which is the ratio of 5% breakthrough time to the

50% breakthrough time. The TPR decreased from 0.93 to 0.87 as the superficial velocity increased from Vs to 2Vs indicating a relatively shallower breakthrough while it increased to 0.94 when the superficial velocity decreased to Vs/2 indicating a relatively steeper breakthrough [49]. This is because the lower is the superficial velocity; the longer is the contact time and the more efficient is the mass transfer. These results are consistent with previous findings[50-52].

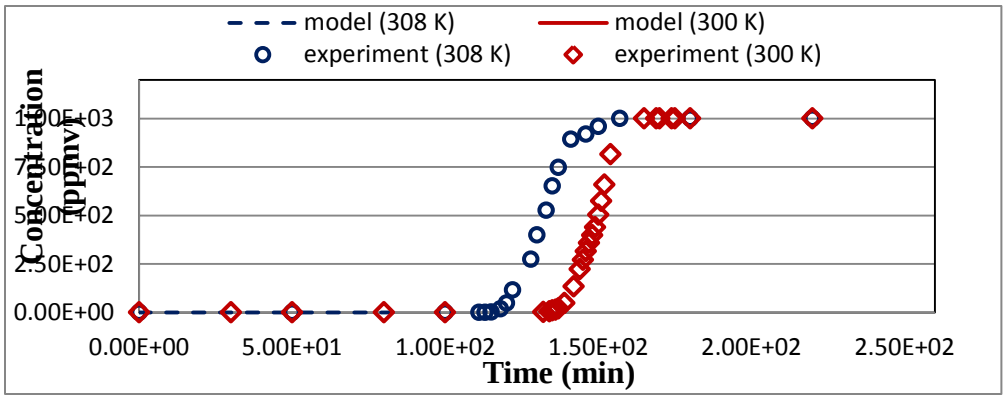

a

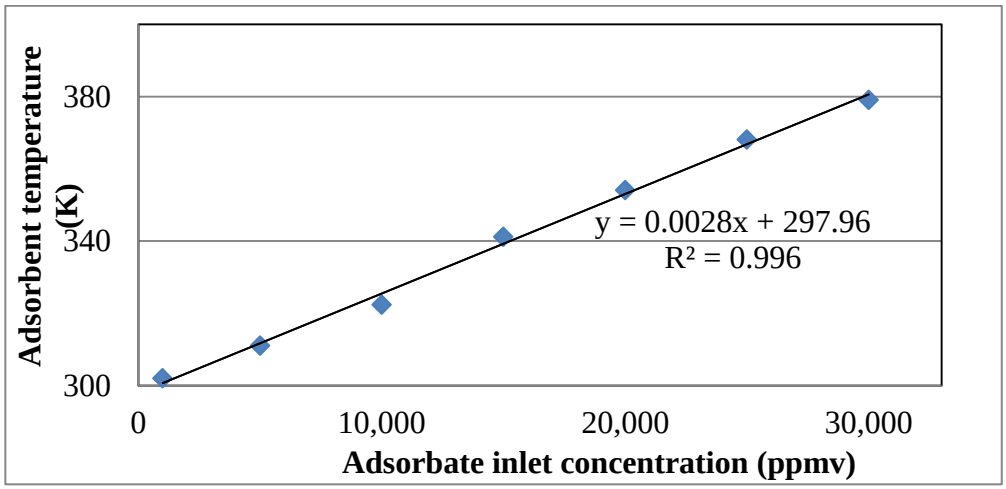

b

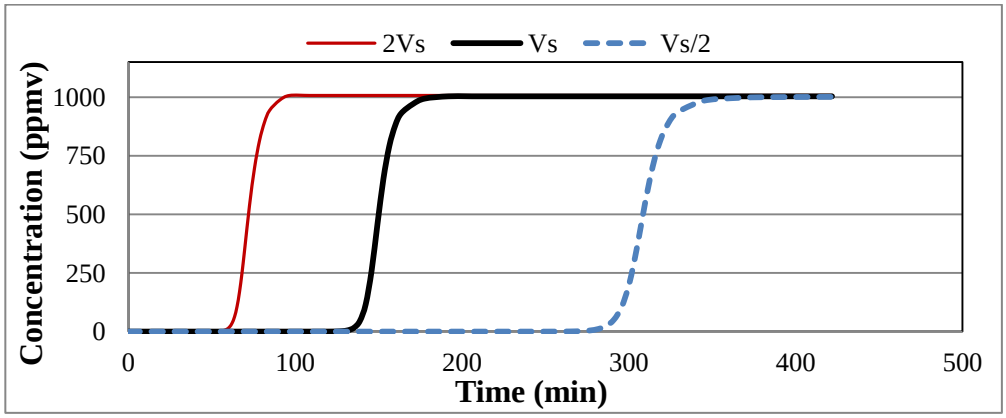

c

Figure 2.6 (a) Effect of carrier gas temperature on benzene breakthrough, (b) modeled effect of inlet benzene concentration on bed temperature, and (c) modeled effect of superficial velocity on benzene breakthrough curve

2.4.6.2 Effect of Particle Size

Activated carbon adsorbents are characterized by their micropores into which the adsorbate molecules need to diffuse. As the adsorbent particle size increases, the mass transfer resistance increases since the adsorbate needs to travel a longer path to reach the deepest micropores. Hence some of the adsorbate molecules would penetrate the adsorbent bed before it is saturated, and the breakthrough curve becomes shallower. On the other hand, as the adsorbent particle size decreases, the mass transfer of the adsorbate becomes faster, the overall rate of adsorption becomes higher and the breakthrough curve becomes sharper (Figure 2.7a) resulting in more complete bed utilization, possibly allowing a reduction in operational costs. Further research is still needed to confirm the model results.

The variation in the radial velocity as a result of variation in the radial bed porosity is related to the adsorbent particle size. The maximum radial velocity was obtained at about one particle diameter from the wall of the reactor due to channelling (Figure 2.7 b) which is also consistent with previous measurements [46]. Reducing the particle size by half reduces the channeling effect while doubling the particle size increases the channelling effect (Figure 2.7b).

Decreasing particle size increases the bed utilization efficiency which will decrease adsorbent or servicing costs but increases the pressure drop and energy consumption. The pressure drop increases because the bulk bed porosity decreases and the flow resistance through the bed increases. Increasing particle size has the opposite effect (Figure 2.7c).

The results obtained in this paper are encouraging as they show that the model can accurately predict the mass, heat, and momentum transfer using adsorbate and adsorbent properties (without the need for fitting parameters) and the adsorber's operating conditions. Hence the model could be used to optimize operational parameters and the adsorbent material during the design of an adsorber in order to minimize overall operational costs.

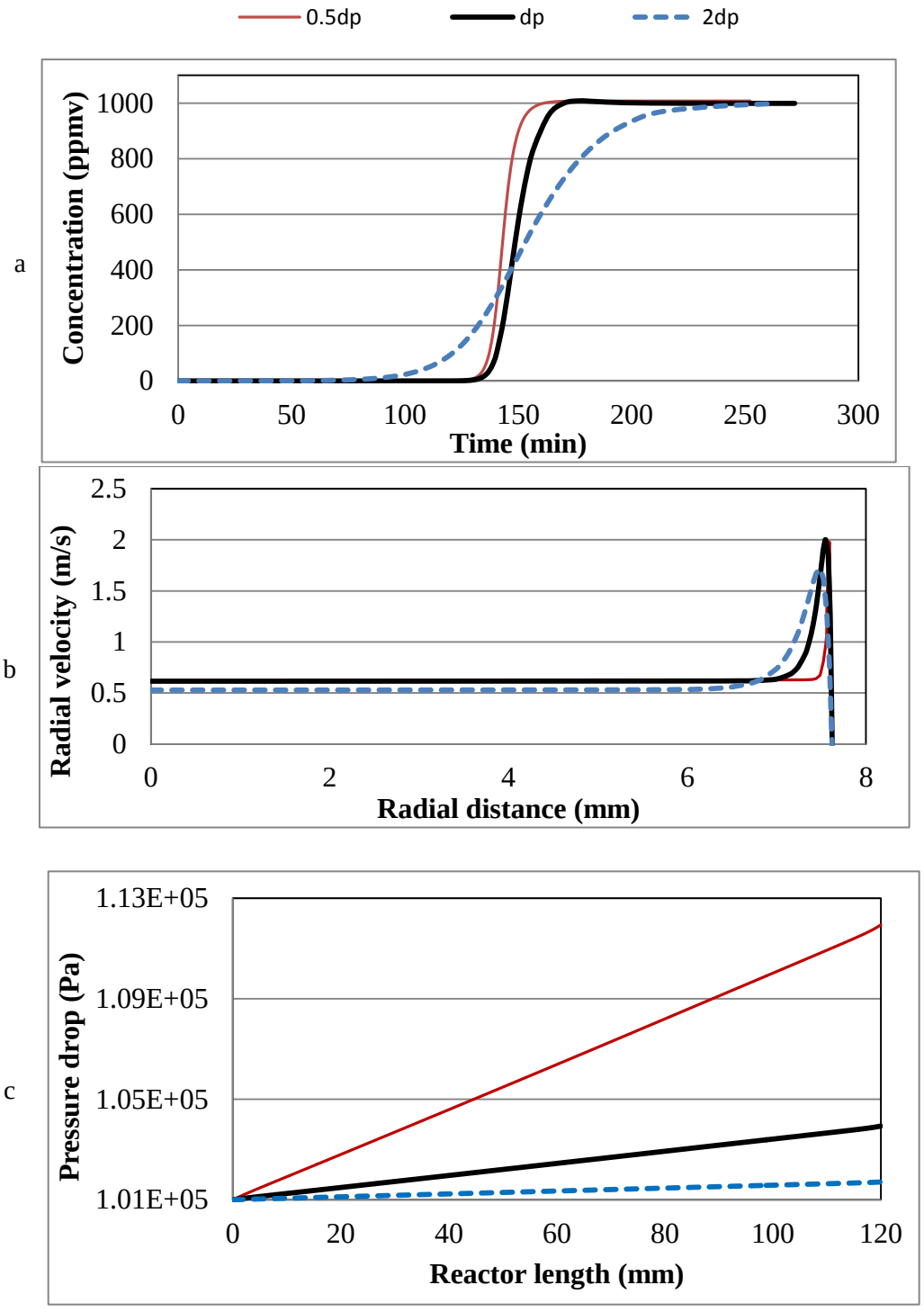

Figure 2.7. Effect of halving and doubling the adsorbent particle size (base case, dp = 0.75mm) on adsorption dynamics of benzene: (a) breakthrough profile; (b) radial velocity profile at the mass transfer zone; and (c) bed pressure drop

2.5 References

1. Hunter, P.; Oyama, S. T., *Control of Volatile Organic Compound Emissions: Conventional and Emerging Technologies*. Wiley: New York **2000**.
2. Parmar, G. R.; Rao, N. N., Emerging control technologies for volatile organic compounds. *Critical Reviews in Environmental Science and Technology* **2009,** *39*, (1), 41-78.
3. Fournel, L.; Mocho, P.; Brown, R.; Le Cloirec, P., Modeling breakthrough curves of volatile organic compounds on activated carbon fibers. *Adsorption* **2010,** *16*, (3), 147-153.
4. Joly, A.; Perrard, A., Linear driving force models for dynamic adsorption of volatile organic compound traces by porous adsorbent beds. *Mathematics and Computers in Simulation* **2009,** *79*, (12), 3492-3499.
5. Murillo, R.; García, T.; Aylón, E.; Callén, M. S.; Navarro, M. V.; López, J. M.; Mastral, A. M., Adsorption of phenanthrene on activated carbons: Breakthrough curve modeling. *Carbon* **2004,** *42*, (10), 2009-2017.
6. Puértolas, B.; López, M. R.; Navarro, M. V.; López, J. M.; Murillo, R.; García, T.; Mastral, A. M., Modelling the breakthrough curves obtained from the adsorption of propene onto microporous inorganic solids. *Adsorption Science and Technology* **2010,** *28*, (8-9), 761-775.
7. Chuang, C. L.; Chiang, P. C.; Chang, E. E., Modeling VOCs adsorption onto activated carbon. *Chemosphere* **2003,** *53*, (1), 17-27.
8. Benenati, R. F.; Brosilow, C. B., Void fraction distribution in beds of spheres. *AIChE Journal* **1962,** *8*, (3), 359-361.
9. Vortmeyer, D.; Winter, R. P., Improvement in reactor analysis incorporating porosity and velocity profiles. *German hemical ngineering* **1984,** *7*, (1), 19-25.
10. Schwartz, C. E.; Smith, J. M., Flow Distribution in Packed Beds. *Industrial & Engineering Chemistry* **1953,** *45*, (6), 1209-1218.
11. Cohen, Y.; Metzner, A. B., Wall effects in laminar flow of fluids through packed beds. *AIChE Journal* **1981,** *27*, (4), 705-715.
12. Mohamadinejad, H.; Knox, J. C.; Smith, J. E., Experimental and umerical nvestigation of wo-Dimensional CO2 dsorption/esorption in acked orption eds nder on-ideal lows. *Separation Science and Technology* **2003,** *38*, (16), 3875-3904.
13. Daszkowski, T.; Eigenberger, G., A reevaluation of fluid flow, heat transfer and chemical reaction in catalyst filled tubes. *Chemical Engineering Science* **1992,** *47*, (9–11), 2245-2250.
14. Cohen, Y.; Metzner, A. B., Wall effects in laminar flow of fluids through packed beds. *AIChE Journal* **1981,** *27*, (5), 705-715.
15. Yin, F.; Wang, Z.; Afacan, A.; Nandakumar, K.; Chuang, K. T., Experimental studies of liquid flow maldistribution in a random packed column. *Canadian Journal of Chemical Engineering* **2000,** *78*, (3), 449-457.
16. Wang, H.; Jahandar Lashaki, M.; Fayaz, M.; Hashisho, Z.; Philips, J. H.; Anderson, J. E.; Nichols, M., Adsorption and desorption of mixtures of

organic vapors on beaded activated carbon. *Environmental Science and Technology* **2012,** *46*, (15), 8341-8350.
17. Lashaki, M. J.; Fayaz, M.; Wang, H.; Hashisho, Z.; Philips, J. H.; Anderson, J. E.; Nichols, M., Effect of adsorption and regeneration temperature on irreversible adsorption of organic vapors on beaded activated carbon. *Environmental Science and Technology* **2012,** *46*, (7), 4083-4090.
18. Nield, D. A.; Bejan, A. Nield, D.A; Bejan. A. Convection in orous edia; Springer: New York, 2006.
19. Dantas, T. L. P.; Luna, F. M. T.; Silva Jr, I. J.; Torres, A. E. B.; De Azevedo, D. C. S.; Rodrigues, A. E.; Moreira, R. F. P. M., Modeling of the fixed-bed adsorption of carbon dioxide and a carbon dioxideitrogen mixture on zeolite 13X. *Brazilian Journal of Chemical Engineering* **2011,** *28*, (3), 533-544.
20. Sircar, S.; Hufton, J. R., Why does the linear driving force model for adsorption kinetics work? *Adsorption* **2000,** *6*, (2), 137-147.
21. Farooq, S.; Ruthven, D. M., A comparison of linear driving force and pore diffusion models for a pressure swing adsorption bulk separation process. *Chemical Engineering Science* **1990,** *45*, (1), 107-115.
22. Sircar, S.; Hufton, J. R., Intraparticle adsorbate concentration profile for linear driving force model. *AIChE Journal* **2000,** *46*, (3), 659-660.
23. Liaw, C. H.; Wang, J. S. P.; Greenkorn, R. A.; Chao, K. C., Kinetics of fixed-bed adsorption - new solution. *AIChE Journal* **1979,** *25*, (2), 376-381.
24. Başağaoğlu, H.; Ginn, T. R.; McCoy, B. J.; Marino, M. A., Linear driving force approximation to a radial diffusive model. *AIChE Journal* **2000,** *46*, (10), 2097-2105.
25. Giraudet, S.; Pré, P.; Le Cloirec, P., Modeling the heat and mass transfers in temperature-swing adsorption of volatile organic compounds onto activated carbons. *Environmental Science and Technology* **2009,** *43*, (4), 1173-1179.
26. Raghavan, N. S.; Hassan, M. M.; Ruthven, D. M., Numerical simulation of a PSA system using a pore diffusion model. *Chemical Engineering Science* **1986,** *41*, (11), 2787-2793.
27. Do, D. D.; Rice, R. G., Revisiting approximate solutions for batch adsorbers: explicit half time. *AIChE Journal* **1995,** *41*, (2), 426-429.
28. Hartzog, D. G.; Sircar, S., Sensitivity of PSA process performance to input variables. *Adsorption* **1995,** *1*, (2), 133-151.
29. Jiang, L.; Biegler, L. T.; Fox, V. G., Simulation and optimization of pressure-swing adsorption systems for air separation. *AIChE Journal* **2003,** *49*, (5), 1140-1157.
30. Logan, D. A., Estimating physical properties for control equipment design. *Environmental Progress* **1997,** *16*, (4), 237-242.
31. Shi, Y.; Lee, Y. T.; Kim, A. S., Knudsen Diffusion Through Cylindrical Tubes of Varying Radii: Theory and Monte Carlo Simulations. *Transport in Porous Media* **2012,** *93*, (3), 517-541.
32. Giraudet, S.; Pŕ, P.; Le Cloirec, P., Modeling the temperature dependence of adsorption equilibriums of VOC(s) onto activated carbons. *Journal of Environmental Engineering* **2010,** *136*, (1), 103-111.

33. Giraudet, S.; Pré, P.; Tezel, H.; Le Cloirec, P., Estimation of adsorption energies using the physical characteristics of activated carbons and the molecular properties of volatile organic compounds. *Carbon* **2006,** *44*, (12), 2413-2421.
34. Smith, J. M.; Van Ness, H. C.; Abbott, M. M., *Introduction to hemical ngineering hermodynamics*. 7th ed.; McGraw-Hill: Boston, 2005; p xviii, 817 p.
35. Bowen, D. H. M., HIST 15-Perry's eavyweight andbook for hemical ngineers. *Abstracts of Papers of the American Chemical Society* **2008,** *236*.
36. Kannuluik, W. G.; Carman, E. H., The emperature ependence of the hermal onductivity of ir. *Australian Journal of Scientific Research Series a-Physical Sciences* **1951,** *4*, (3), 305-314.
37. Kuwagaki, H.; Meguro, T.; Tatami, J.; Komeya, K.; Tamura, K., An improvement of thermal conduction of activated carbon by adding graphite. *Journal of Materials Science* **2003,** *38*, (15), 3279-3284.
38. Bey, O.; Eigenberger, G., Gas flow and heat transfer through catalyst filled tubes. *International Journal of Thermal Sciences* **2001,** *40*, (2), 152-164.
39. Kwapinski, W., Combined wall and thermal effects during non-isothermal packed bed adsorption. *Chemical Engineering Journal* **2009,** *152*, (1), 271-276.
40. Oliemans, R. V. A., ERCOFTAC's role in promoting computational fluid dynamics. *Houille Blanche* **2000**, (7-8), 43-46.
41. Hutton, A. G., Quality and trust in industrial computational fluid dynamics. **2001**, (3-4), 25-28.
42. Oberkampf, W. L.; Trucano, T. G., Verification and validation in computational fluid dynamics. *Progress in Aerospace Sciences* **2002,** *38*, (3), 209-272.
43. Jahandar Lashaki, M.; Fayaz, M.; Niknaddaf, S.; Hashisho, Z., Effect of the adsorbate kinetic diameter on the accuracy of the Dubinin-Radushkevich equation for modeling adsorption of organic vapors on activated carbon. *Journal of Hazardous Materials* **2012,** *241-242*, 154-163.
44. Williams, L. E.; Barnett, M. O.; Kramer, T. A.; Melville, J. G., Adsorption and transport of arsenic(V) in experimental subsurface systems. *Journal of Environmental Quality* **2003,** *32*, (3), 841-850.
45. Chahbani, M. H.; Tondeur, D., Pressure drop in fixed-bed adsorbers. *Chemical Engineering Journal* **2001,** *81*, (1-3), 23-34.
46. Negrini, A. L.; Fuelber, A.; Freire, J. T.; Thoméo, J. C., Fluid dynamics of air in a packed bed:velocity profiles and the continuum model assumption. *Brazilian Journal of Chemical Engineering* **1999,** *16*, (4), 421-432.
47. Breugem, W. P., The effective viscosity of a channel-type porous medium. *Physics of Fluids* **2007,** *19*, (10).
48. Pré, P.; Delage, F.; Faur-Brasquet, C.; Le Cloirec, P., Quantitative structure-activity relationships for the prediction of VOCs adsorption and desorption energies onto activated carbon. *Fuel Processing Technology* **2002,** *77-78*, 345-351.

49. Hashisho, Z.; Rood, M.; Botich, L., Microwave-swing adsorption to capture and recover vapors from air streams with activated carbon fiber cloth. *Environmental Science and Technology* **2005,** *39*, (17), 6851-6859.
50. Chern, J. M.; Chien, Y. W., Adsorption of nitrophenol onto activated carbon: isotherms and breakthrough curves. *Water Research* **2002,** *36*, (3), 647-655.
51. Pan, B. C.; Meng, F. W.; Chen, X. Q.; Pan, B. J.; Li, X. T.; Zhang, W. M.; Zhang, X.; Chen, J. L.; Zhang, Q. X.; Sun, Y., Application of an effective method in predicting breakthrough curves of fixed-bed adsorption onto resin adsorbent. *Journal of Hazardous Materials* **2005,** *124*, (1-3), 74-80.
52. Mark M. Benjamin, D. F. L., *Water Quality Engineering: Physical / Chemical Treatment Processes*. John Wiley & Sons: Inc., Hoboken, New Jersey, 2013.

CHAPTER 3 MODELING COMPETITIVE ADSORPTION OF MIXTURES OF VOLATILE ORGANIC COMPOUNDS (VOCS) ONTO BEADED ACTIVATED CARBON (BAC)

A version of this chapter will be submitted for publication. Reproduced with permission from Dereje Tamiru Tefera**,** Zaher Hashisho, John H. Philips, James E. Anderson, Mark Nichols

3.1 Introduction

Painting booths are the main source of volatile organic compounds (VOCs) in the automotive industry [1,2]. These emissions originate from the use of solvent-based and waterborne paints and consists of a complex mixture of organic vapours with wide range of functional groups, boiling point, and volatility [3]. VOCs from automotive painting operations are often sent to an abatement system to reduce their potential impact on public health and the environment before discharge to the atmosphere [4]. Adsorption on a fixed bed of activated carbon is a commonly used abatement method for capturing VOCs emissions from industrial gas streams. Multicomponent adsorption involves both the interactions among the adsorbates and the adsorbate-adsorbent interactions, with the complexity of multicomponent adsorption increasing as the number of components in the mixture increases [5]. One of the most important adsorbate-adsorbate interactions in multicomponent adsorption is competition for the active adsorption sites. In competitive adsorption, a component with stronger affinity to the adsorbent will preferentially adsorb and can reduce the adsorbed phase concentration of the component with weaker affinity [6]. In a fixed bed adsorber, the effects of competitive adsorption are observed as a component with weaker affinity showing an increase in outlet concentration above its inlet concentration as it is displaced from the adsorbed phase by a second component with stronger affinity [3]. Because experimental study of multicomponent adsorption is usually expensive and time-consuming, development of mathematical models to predict multicomponent adsorption is very important for better understanding of the process, and for

proper design, analysis and optimization of fixed bed adsorbers for VOCs emission control.

A comprehensive model for the adsorption process consists of a model for the analysis of dynamic adsorption (macroscopic mass, energy and momentum conservation equations) coupled to a model of equilibrium adsorption (isotherm equations). Previous studies on modelling dynamic adsorption of competing adsorbates focused on binary [6, 7 8] or ternary [9, 10] mixtures. However, most industrial emissions usually consist of mixture of more than three adsorbates, as is the case of emissions from automotive painting booths [3,1]. Hence, there is a need for developing a mathematical model to predict the multicomponent competitive adsorption of mixtures of any number of adsorbates.

To model equilibrium multicomponent adsorption, the first and the simplest model used was the extended Langmuir isotherm equation. The Langmuir isotherm was extended by Butler and Ockrent [11] to predict binary component adsorption with the same assumption that Langmuir made for single-component adsorption. The Langmuir isotherm was then extended to predict equilibrium adsorption of multicomponent mixtures [12]. Due to discrepancies of the extended Langmuir isotherm model seen for concentrated feed systems, various investigators developed different multicomponent isotherm models such as isotherms based on ideal adsorbed solution theory and real adsorbed solution theory [12] as well as isotherm models based on potential theory [13]. Jain and Snoeyink [14] demonstrated the limitation of extending single-component Langmuir isotherms to competitive adsorption of binary systems and proposed a new form

of competitive isotherm model, called the modified Langmuir-like equation, for binary mixtures of organic compounds in wastewater. A similar model was then developed for the prediction of competitive adsorption of a ternary mixture from liquid stream [15]. These models are computationally simple and showed very good prediction capability for low concentration streams but are limited to ternary component mixtures. In the current work, a new n-component adsorption model similar to Jain and Snoeyink's model was derived to predict the competitive adsorption isotherm of any n-component VOCs mixture from the gas phase, with n limited only by computational capability.

The goal of this research is to develop a fully predictive mathematical model to study the competitive adsorption of a mixture of VOCs. This will be achieved by developing: 1) a multicomponent competitive adsorption isotherm model that can predict equilibrium adsorption of an n-component VOCs mixture using single-component isotherm parameters; 2) a fully predictive two-dimensional mathematical model for the transport of mass, energy and momentum during the competitive adsorption of the n-component VOCs mixture onto a fixed bed of beaded activated carbon.

3.2 Model Development and Validation

3.2.1 Physical Model

The bench scale adsorber used to validate the model consisted of a cylindrical reactor with a 0.76 cm inner radius (R) loaded with 7.16 g of beaded activated carbon (BAC) particles (mean diameter = 0.75 mm) resulting in a net bed length

(L) of 6.5 cm. A 10 SLPM air stream containing 500 ppmv of the test adsorbates entered from the top of the reactor at a superficial velocity of 0.914 m/s and exited from the bottom of the reactor. The flow field was calculated using 2-dimensional axisymmetric geometry to reduce the computational time. Major assumptions made include: negligible variation of flow properties in the angular direction; negligible adsorption of the carrier gas; ideal gas behavior; and symmetric flow conditions.

3.3 Governing Transport Phenomena

The model is based on the concept that the fixed bed adsorber consists of two-phases, the mobile (gas) phase and the immobile (solid adsorbent) phase where mass transfer of adsorbate is described by advection-dispersion and by diffusion in the gas and solid phases, respectively. The multi-component transport model was developed by extending a validated single-component transport model [16] to n-components coupled with a new competitive adsorption isotherm model. Table 3.1 provides the definitions and equations for the model variables and parameters.

1.1.1 Mass Balance for the Gas Phase

The convection-dispersion mass transfer equation for the transport of multiple adsorbates in the gas phase (i^{th} component) is:

$$\varepsilon_r \frac{\partial C_i}{\partial t} - \nabla(D_i \varepsilon_r \nabla c_i) + \nabla(u c_i) + S_{m,i} = 0 \quad \text{.....3.1}$$

3.3.2 Mass Balance for the Solid Phase

The diffusive adsorbate transport in the solid phase is approximated using the linear driving force (LDF) model [17] [18].

$$\frac{\partial C_{s,i}}{\partial t} = k_{ov,i}(c_{se,i} - c_{s,i}) = S_{m,i} \quad \text{.....3.2}$$

3.3.3 Multicomponent Competitive Adsorption Isotherm

A competitive adsorption isotherm model (equation 3.3) was derived to predict the equilibrium adsorption of the n-component adsorbate mixture using single-component isotherm parameters. Derivation of the competitive adsorption isotherm equation is provided in the Appendix A .

$$q_{e,i} = \sum_{k=i}^{n} \frac{b_i c_i a_k}{1+\left(\sum_{j=1}^{k} b_j c_j\right)} \quad \text{.....3.3}$$

Where: $q_{e,i}$ is the equilibrium adsorption capacity of the i^{th} component (i =1 to n);

$a_k=(q_{m,k} - q_{m,k+1})$ for k= i to n-1 and $a_k = q_{m,n}$, for k = n

b_j is the affinity coefficient [19] where j=1 to k

$$b_j = b_{o,j} \exp\left(\frac{-\Delta H_{ad,j}}{R_g T}\right) \quad \text{.....3.4}$$

Equation 3 was coupled with the mass transfer model (equations 3.1 and 3.2) to model the competitive adsorption of both a binary mixture and an eight component mixture of VOCs.

3.3.4 Energy Balance

The energy balance assumes local thermal equilibrium between the solid and gas phase; and negligible viscous heat dissipation and pressure work. Hence, convection- diffusion heat transport was used [20].

$$C_v \frac{\partial T}{\partial t} + C_{pf}\rho_f u.\nabla T - \nabla.(k_{ef}\nabla T) = \sum_i^n S_{h,i} \ldots \quad 3.5$$

The domain heat source due to the adsorption of the i^{th} component, neglecting the viscous dissipation, is given as:

$$S_{h,i} = \left(-\Delta H_{ad,i}\right)\frac{dc_{s,i}}{dt} \quad 3.6$$

3.3.5 Momentum Balance

A modified momentum balance equation (equation 3 7) which accounts for Darcy and Brinkman viscous terms, Forchheimer's inertial term, and Navier–Stokes' convective term[20] was used to model the non-Darcy gas flow of multicomponent VOCs in the fixed bed adsorber.

$$\frac{\rho_f}{\varepsilon_r}\left(\left(\frac{\partial u}{\partial t}\right) + (u.\nabla)\frac{u}{\varepsilon_r}\right) = -\nabla P + \nabla.J - S + F \quad 3.7$$

The shear stress is defined in terms of fluid viscosity (equation 3.8).

$$J = \left(\frac{1}{\varepsilon_r}\left(\mu_f \nabla u + (\nabla u)^T - \frac{2}{3}\mu_f(\nabla . u)I\right)\right) \quad \text{.....3.8}$$

Momentum dissipation of the flow in the fixed-bed adsorber is accounted for by Darcy's friction loss factor, Forchheimer's inertial term, and a sink term due to the adsorption of the n components (equation 3.9).

$$S = \left(\frac{\mu_f}{K} + \beta|v| + \frac{\sum_{i=1}^{n} S_{m,i}}{\varepsilon_r}\right) u \quad \text{.....3.9}$$

The continuity equation accounts for the compressibility of the fluid and the sink due to the adsorption of the n components (equation 3.10).

$$\frac{\partial(\varepsilon\rho_f)}{\partial t} + \nabla . (\rho_f u) = \sum_{i=1}^{n} S_{m,i} \quad \text{.....3.10}$$

3.3.6 Variable and parameters definition

Table 3.1 shows the definition of the model variables and parameters.

Table 3.1 Model variables and parameters

Symbol	Description	Value /Formula	Units	Source
$\mathbf{b_j}$	Temperature-dependent Langmuir affinity coefficient	Equation 3.4	m^3/kg	[19]
$\mathbf{b_{o,j}}$	Pre-exponential constant in Langmuir isotherm	Table 3.3	m^3/kg	Equation 3.15
$\mathbf{c_i}$	Gas phase concentration	Equation 3.1	kg/m^3	N/A
$\mathbf{C_F}$	Empirical correction factor for Forchheimer's drag coefficient calculation	$0.55\left(1-5.5\left(\frac{d_p}{D_b}\right)\right)$	1	[20]
$\mathbf{c_{o,i}}$	Inlet gas concentration	250 for binary mixture, 62.5 for eight-component mixture	ppmv	Table 3.2
$\mathbf{c_{s,\,i}}$	Adsorbed phase concentration	Equation 3.2	kg/m^3	[17]
$\mathbf{c_{se,\,i}}$	Equilibrium adsorbed phase concentration	$\rho_b q_{e,i}$	kg/m^3	N/A
$\mathbf{c_{so,i}}$	Adsorbed phase concentration in equilibrium with inlet gas phase concentration	$\rho_b q_{m,i}$	kg/m^3	N/A
$\mathbf{C_{pf}}$	Gas heat capacity	$286.9(3.33 + 0.000575T^2 - 1600/T^2)$ (air)	J/kg.K	[21]
$\mathbf{C_{pp}}$	Adsorbent heat capacity	706.7 (BAC)	J/kg.K	[22]
$\mathbf{C_v}$	Effective volumetric heat capacity of the solid-gas system	$(1-\varepsilon_b)\rho_p C_{pp}+\varepsilon_b \rho_f C_{pf}$	$J/(m^3.K)$	[20]
$\mathbf{D_i}$	Symmetric mass dispersion tensor	$\begin{vmatrix} D_{r,i} & 0 \\ 0 & D_{ax,i} \end{vmatrix}$	cm^2/s	N/A

$\mathbf{D_{AB,i}}$	Molecular diffusivity	$\frac{10^{-3}T^{1.75}\sqrt{\frac{M_{A,i}+M_B}{M_{A,i}M_B}}}{P\left((\sum v)_{A,i}^{0.33}-(\sum v)_B^{0.33}\right)^2}$	cm^2/s	[23]
$\mathbf{D_{ax,i}}$	Axial dispersion coefficient	$\left(\alpha_0+\frac{ScRe_p}{2}\right)\frac{D_{AB,i}}{\varepsilon_b}$	cm^2/s	[24]
$\mathbf{D_b}$	Reactor inner diameter	0.0152	m	Measured
$\mathbf{D_{eff,i}}$	Effective diffusion coefficient	$\frac{1}{D_{eff,i}}=\frac{1}{D_{AB,i}}+\frac{1}{D_{k,i}}$	cm^2/s	[25]
$\mathbf{D_{k,i}}$	Knudsen diffusivity	$9700r_p\sqrt{\frac{T}{M_{A,i}}}$	cm^2/s	[26]
$\mathbf{d_p}$	Average adsorbent particle diameter	$7.5x10^{-4}$ (BAC)	m	[27]
$\mathbf{D_{r,i}}$	Radial dispersion coefficient	$\left(\alpha_0+\frac{ScRe_p}{8}\right)\frac{D_{AB,i}}{\varepsilon_b}$	m^2/s	[28]
F	Body force	$g\boldsymbol{\rho_f}$	N/m^3	[20]
g	Acceleration of gravity	9.81	m/s^2	
$\mathbf{\Delta H_{ad,i}}$	Heat of adsorption	$103.2+1.16\alpha_i+0.76\Delta H_{vap,i}-3.87(IP_i)-0.7\gamma_i-26.1w_{mic}$	kJ/mol	[29]
$\mathbf{\Delta H_{vap,i}}$	Adsorbate heat of vaporization	Table B.1	kJ/mol	Appendix B
I	Unit vector	N/A		N/A
J	Shear stress	Equation 3.8	N/m^2	N/A
K	Bed permeability	$\frac{\varepsilon_b{}^3 d_p{}^2}{150(1-\varepsilon_b)^2}$	m^2	[20]
$\mathbf{k_{ax}}$	Axial thermal diffusion coefficient	$K_b+\frac{1}{2}Pe_o k_f$	W/m.K	[30]
$\mathbf{k_b}$	Stagnant bed thermal conductivity	$(1-\varepsilon_b)k_p+\varepsilon_b k_f$	W/m.K	[30]
$\mathbf{k_{ef}}$	Symmetric thermal diffusion	$\begin{vmatrix} K_r & 0 \\ 0 & K_{ax} \end{vmatrix}$	W/m.K	N/A

	coefficient			
$\mathbf{k_f}$	Gas thermal conductivity	$1.521 \times 10^{-11}T^3 - 4.8574 * 10^{-8}T^2 + 1.084 * 10^{-4} - 0.0003939333$ (Air)	W/m.K	[31]
$\mathbf{k_{ov,i}}$	Overall mass transfer coefficient	$\frac{60\varepsilon_p C_{o,i} D_{eff,i}}{\tau_p C_{so,i} {d_p}^2}$	1/s	[28]
$\mathbf{k_p}$	Adsorbent particle thermal conductivity	0.17 (BAC)	W/m.K	[32]
$\mathbf{k_r}$	Radial thermal diffusion coefficient	$K_b + \frac{1}{8} Pe_o k_f$	W/m.K	[30]
$\mathbf{k_w}$	Wall heat transfer coefficient	$\frac{2.4}{d_p} K_{bed} + 0.054 \frac{K_f}{d_p} \left(1 - \frac{d_p}{D_b}\right) Re_p {P_r}^{1/3}$	1	[33]
$\mathbf{IP_i}$	Ionization potential	Table B 1	eV	Appendix B
$\mathbf{M_{A,i}}$	Molecular weight	Table B 1	g/mol	[3]
$\mathbf{M_B}$	Gas molecular weight	29 (Air)	g/mol	
P	Gas pressure	Equation 3.7	Pa	N/A
$\mathbf{Pe_o}$	Molecular Peclet number for heat transfer	$\frac{V_s \rho_f C_{pf} d_p}{K_f}$	1	[30]
$\mathbf{p_r}$	Prandtl number	$\frac{\mu_f C_{pf}}{k_f}$	1	[33]
$\mathbf{q_{e,i}}$	Adsorbent equilibrium capacity	Equation 3.3	g/g	N/A
$\mathbf{q_{m,i}}$	Adsorbent maximum capacity	Table 3.3	g/g	Calculated
r	Radial distance	Variable	m	N/A
R	Radius of the adsorber	$\frac{D_b}{2}$	m	N/A
$\mathbf{Re_p}$	Particle Reynolds number	$\frac{\rho_f V_s d_p}{\mu_f}$	1	[28]
$\mathbf{R_g}$	Ideal gas constant	8.314	J/(mol.K)	
S	Momentum sink	Equation 9	N/ m^3	N/A

	due to adsorption			
$\mathbf{Sc_i}$	Schmidt number	$\frac{\mu_f}{\rho_f D_{AB,i}}$	1	[28]
$\mathbf{S_{h,i}}$	Heat source due to adsorption	Equation 3.6	J/(m^3.s)	N/A
$\mathbf{S_{m,i}}$	Mass sink due to adsorption	Equation 3.2	kg/(m^3.s)	N/A
t	Adsorption time	Variable	s	N/A
T	Temperature	Equation 3.5	K	N/A
$\mathbf{T_{inlet}}$	Gas inlet temperature	300	K	(BC2)
$\mathbf{T_w}$	Adsorber wall temperature	295	K	(BC2)
u	Gas flow velocity vector	Equation 3.7	m/s	N/A
|v|	Resultant velocity	Equation 3.9	m/s	N/A
$\mathbf{V_{pore}}$	Adsorbent pore volume	0.57 (BAC)	cm^3/g	Measured
$\mathbf{V_s}$	Superficial velocity	0.914	m/s	Table 3.2
$\mathbf{w_{mic}}$	Adsorbent average micropore width	1.02 (BAC)	nm	Measured
Z	Axial distance	Variable	m	N/A

Greek Symbols

Parameter	Description	Value /equation	Unit	Source
$\boldsymbol{\alpha_i}$	Polarizability	Table B 1	cm^{3}x10^{-24}	Appendix B
$\boldsymbol{\alpha_0}$	Empirical correction factor for mass diffusion terms	20	1	[28]
$\boldsymbol{\beta}$	Forchheimer's drag coefficient	$\rho_f \frac{C_F}{\sqrt{K}}$	kg/m^4	[20]
γ_i	Surface tension	Table B 1	mN/m	Appendix B
$\boldsymbol{\varepsilon_b}$	Bulk bed porosity	$0.379 + \frac{0.078}{\left(\frac{D_b}{d_p}\right)-1.8}$	1	[20]
$\boldsymbol{\varepsilon_p}$	Particle porosity	$\boldsymbol{\rho_p V_{pore}}$	1	[16]

$\boldsymbol{\varepsilon_r}$	Bed porosity as a function of radial distance from the center	$\varepsilon_b\left(1+\left(\frac{1-\varepsilon_b}{\varepsilon_b}\right)\right.$ $\left.*\exp\left(6\frac{\mathrm{R}-\mathrm{r}}{\mathrm{d_p}}\right)\right)$		[20]
$\mu_\mathbf{f}$	Gas viscosity	Temperature dependent	Pa.s	COMSOL material database
$\boldsymbol{\rho_b}$	Bulk bed density	606	kg/m^3	Measured
$\boldsymbol{\rho_f}$	Gas density	Temperature dependent	kg/m^3	COMSOL material database
$\boldsymbol{\rho_p}$	Adsorbent particles density	$\frac{\boldsymbol{\rho_b}}{\mathbf{1}-\boldsymbol{\varepsilon_b}}$	kg/m^3	[22]
$\boldsymbol{\tau_p}$	Adsorbent particles tortuosity	$\frac{\mathbf{1}}{\boldsymbol{\varepsilon_p}^{\mathbf{2}}}$	1	[34]
$(\sum \mathbf{v})_{\mathbf{A,i}}$	Atomic diffusion volume	Table B 1	1	[23]
$(\sum \mathbf{v})_{\mathbf{B}}$	Atomic diffusion volume of air	20.1	1	[23]

Indices	
i	Component index ranging from 1 to n components
j	Summation index ranging from 1 to k
k	Summation index ranging from i to n
n	Number of adsorbates in the mixture

**N/A: Not applicable

3.3.7 Initial and Boundary Conditions

The initial and boundary conditions used with the model are summarized in

Table **3.2** . For mass transfer, a concentration boundary condition at the inlet and a flux boundary condition at the outlet were used. For heat transfer, a temperature boundary condition at the inlet, a constant flux boundary condition at the outlet, and a convective heat flux at the wall were specified. For momentum balance, a normal velocity boundary condition was set at the inlet and a constant pressure was set at the outlet.

Table 3.2 Initial and boundary conditions

Physics	Inlet (Z=H)	Outlet (Z=0)	Adsorber wall (r=R)	Initial condition
Mass transfer	c_i=$c_{o,i}$ $c_{s,i}$=$c_{so,i}$	Boundary flux $-n.(D\nabla c_i)$=0 and $-n.\left(D\nabla c_{s,i}\right)$ =0	Zero flux	$c_{o,i}$=0 $c_{s,i}$=0
Heat transfer	T=T_{inlet}	$-n.(K\nabla T)$=0	$q_o = k_w(T_w - T)$	T=295K
Momentum transfer	V_s=0.914 m/s	P=1atm	No slip	P=1atm u=0

3.3.8 Method of Solution

Simulation of the coupled mass, energy and momentum balance was performed using COMSOL Multiphysics version 4.3a where the developed governing equations were solved numerically using the finite element method. A second-order element was used for concentration, temperature and pressure while a third-order element was used for velocity to avoid solution instability and enhance convergence [35-37]. Convergence of the solution was confirmed by systematic mesh refinement until a grid-independent solution was obtained. The final solution was presented using a total mesh of 43,868 elements which showed a relative deviation of only 0.80% from the solution obtained by using a finer mesh, 61,898.

3.3.9 Experimental Methods

To validate the model, measured breakthrough concentrations and amounts of adsorbates adsorbed for a binary mixture and an eight-component VOCs mixture from a previous study [3] were used. The modelled scenarios used the same

adsorbent properties and similar experimental conditions as those for the experimental measurements.

The deviation between the modelled and measured breakthrough profiles was evaluated using two error metrics. For non-zero data points, mean relative absolute error (MRAE) [38] was used.

$$\text{MRAE} = \frac{1}{N}\sum_{1}^{N}\left|\frac{|experimental\ value - modelled\ value|}{experimental\ value} * 100\right| \quad \text{.....3.12}$$

Where N is the number of data points compared.

The overall error in predicting the experimental breakthrough profiles was evaluated using the root mean square error (RMSE) normalised by the influent stream concentration [39].

$$\text{RMSE} = \sqrt{\frac{1}{N}\sum_{1}^{N}\left(\frac{experimental\ value - modelled\ value}{influent\ stream\ value}\right)^{2}} * 100 \quad \text{.....3.13}$$

In addition to the comparison to breakthrough concentrations, the model was validated by comparing the modeled amounts of each specie adsorbed on the BAC to the amounts measured by solvent extraction of the BAC following the adsorption as reported in Wang et al.[3].

The prediction of the competitive multicomponent adsorption isotherm is based on single-component adsorption isotherm parameters which were obtained by fitting single-component experimental adsorption isotherm data to the single-component Langmuir isotherm model. Single-component adsorption isotherm data of the VOCs (n-heptane, n-butanol, n-butyl acetate, 2-heptanone, 2-

butoxyethanol, n-decane, indane, 2,2-dimethylpropylbenzene and 1,2,4-trimethylbenzene) were obtained through mass balance on a fixed bed of 4 to 5 g of BAC adsorbing at three different influent VOC concentrations in a 10 SLPM air stream at 25^{o}C. Detailed information about the experimental setup used for the adsorption has been described previously [27, 3]. Adsorption was continued until equilibrium between the gas and the adsorbent was reached as indicated by effluent gas concentration measured using a photoionization detector (Minirae 2000, Rae Systems). Adsorption was stopped 20 min after the measured effluent and influent gas concentrations were equal, to ensure that equilibrium between the gas and solid phases had been reached. The experimental single component adsorption isotherms and the isotherm parameters are provided in the Supporting Information.

3.4 Results and Discussion

3.4.1 Single Component Isotherm Parameters

The pure component Langmuir isotherm parameters were determined by linearizing the corresponding isotherm equation (equation 3.14) and fitting the resulting equation to measured isotherm data Figure 3.1, obtained by completing a mass balance on a reactor loaded with 4 to 5g of BAC and adsorbing at 25^{o}C where air is used as carrier gas. In equation 3.14 the slope of the line is $\left(\frac{1}{b_j q_{mi}}\right)$, the y-intercept is $\left(\frac{1}{q_{mi}}\right)$. Hence, b_j and q_{mi} can be readily calculated at 25^{o}C.

$$\frac{1}{q_{ei}} = \frac{1}{b_j q_{mi} C} + \frac{1}{q_{mi}} \quad \text{.....3.14}$$

Knowing the value of b_j at 25 ^{o}C (using Figure 3.1and equation 3.15), $b_{o,j}$ can be calculated using equation 3.15

$$b_{o,j} = \frac{\boldsymbol{b_j at\ 25℃}}{\boldsymbol{exp}\left(\frac{-\Delta \boldsymbol{H_{ad}}}{\boldsymbol{TR}}\right)} \quad \text{.....3.15}$$

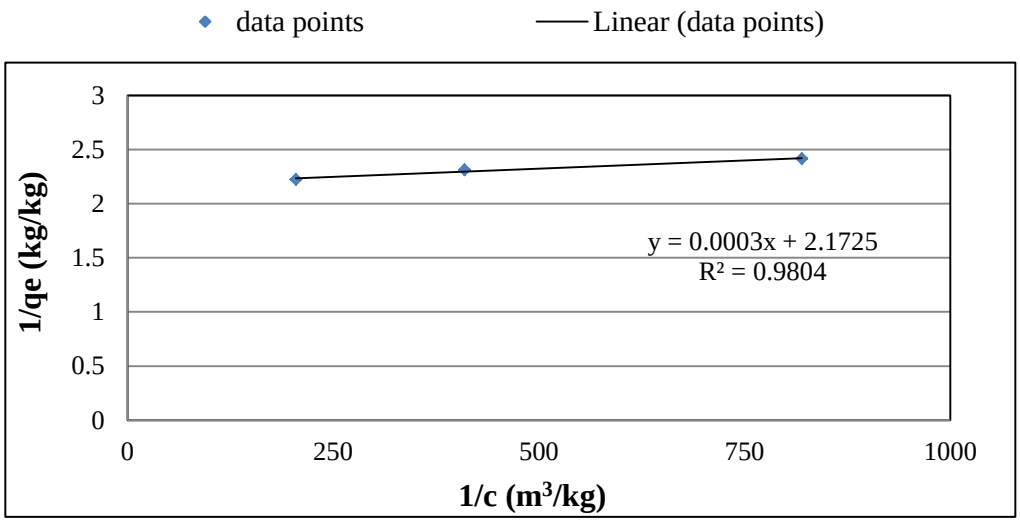
data points
Linear (data points)
1/qe (kg/kg)
y = 0.0003x + 2.1725
R² = 0.9804
1/c (m³/kg)

a

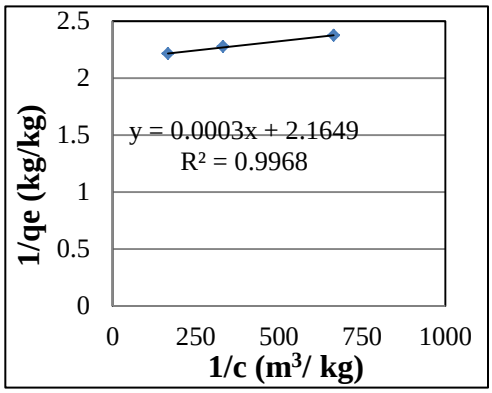
1/qe (kg/kg)
y = 0.0003x + 2.1649
R² = 0.9968
1/c (m³/ kg)

b

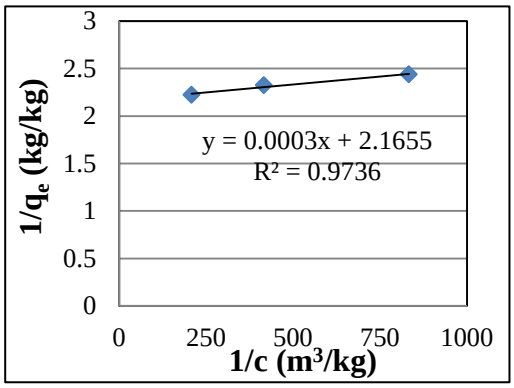
1/qe (kg/kg)
y = 0.0003x + 2.1655
R² = 0.9736
1/c (m³/kg)

c

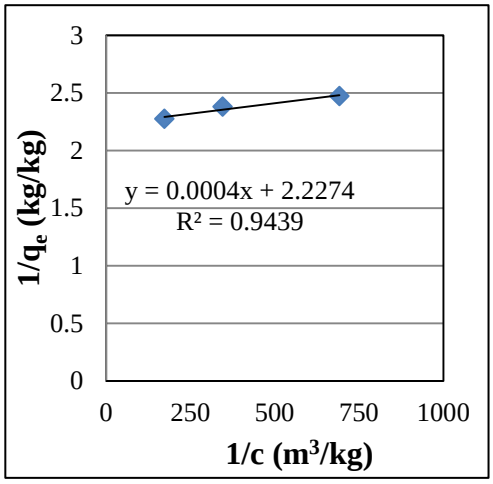
1/qe (kg/kg)
y = 0.0004x + 2.2274
R² = 0.9439
1/c (m³/kg)

d

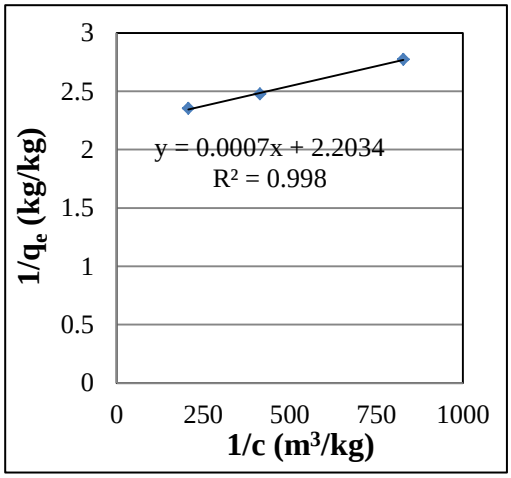
1/qe (kg/kg)
y = 0.0007x + 2.2034
R² = 0.998
1/c (m³/kg)

e

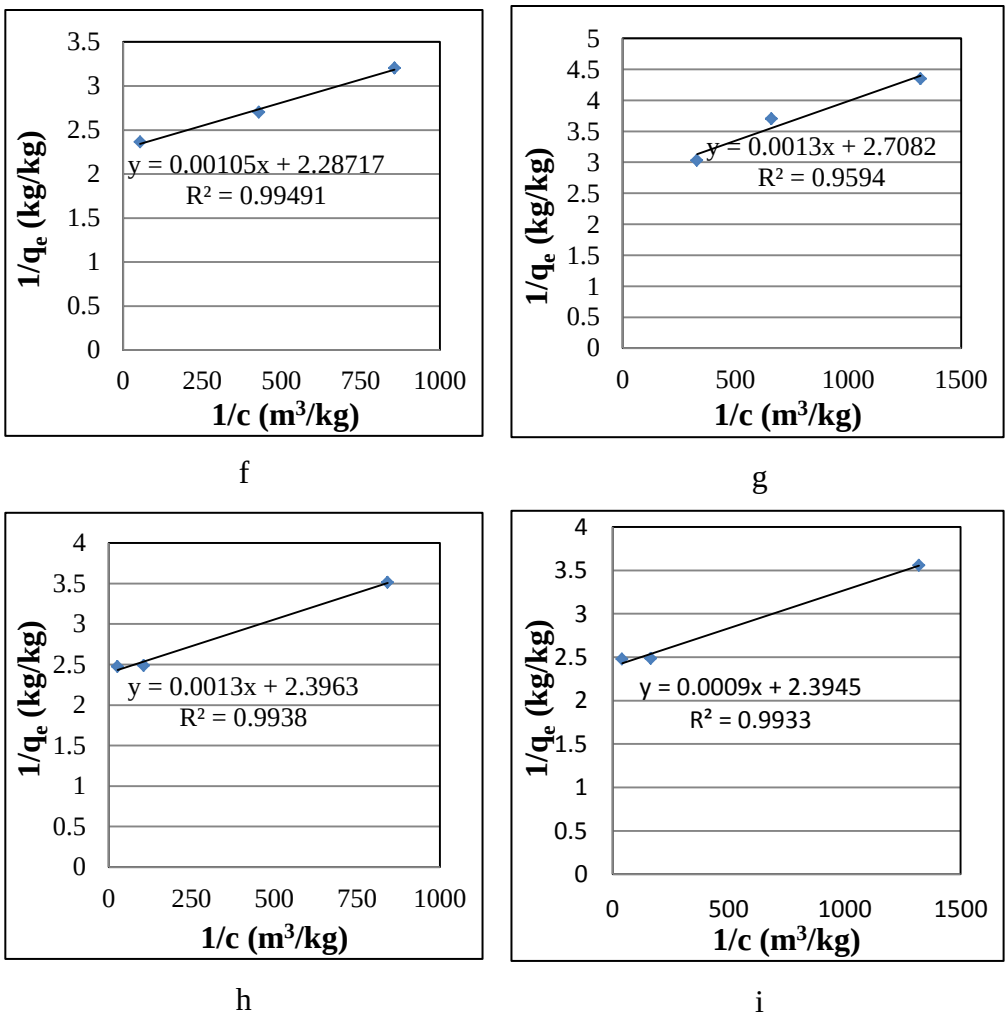

Figure 3.1 Calculation of Langmuir isotherm parameters for individual compounds (a) 1,2,4-trimethylbenzene, (b) 2,2-dimethylpropylbenzene, (c) indane, (d) decane, (e) 2-butoxy ethanol, (f) 2-hepatnone, (g) heptane, (h) n-butyl acetate, and (i) n-butanol.

Table 3.3. shows Langmuir isotherm parameters for each compound: the maximum adsorption capacity ($q_{m,i}$), the Langmuir affinity coefficient at 25^{o}C (b_j at25^{o}C) and the pre-exponential constant in the temperature dependent Langmuir affinity coefficient ($b_{o,j}$).

Table 3.3.Langmuir isotherm parameters

Compound	$q_{m,i}$ (Kg/Kg)	b_j at25°C (m^3/kg)	$b_{o,j}$ (m^3/kg)
1,2,4-trimethylbenzene	0.46	7242	9.73389E-12
2,2-dimethylpropylbenzene	0.46	7216	9.3829E-12
Indane	0.46	5338	8.64472E-13
Decane	0.45	4455	6.08374E-13
2-butoxyethanol	0.45	3148	2.34228E-13
2-heptnone	0.44	2287	1.77605E-13
Heptane	0.37	2083	5.00574E-12
n-butyl acetate	0.42	1843	9.86569E-15
n-butanol	0.42	1710	1.51552E-15

3.4.2 Binary Component (n=2) Adsorption

Figure 3.2a shows the adsorption breakthrough curves of a mixture of n-decane (decane) and n-heptane (heptane) as compared to the experimental result from a previous study [3]. The model predicted the measured breakthrough curves of the binary mixture with a MRAE of 13% and RMSE of 11%. While numerical error and/ or model assumptions could be contributors, the deviation is most likely due to the experimental error in measuring the breakthrough concentrations with tedlar bags and gas chromatography-mass spectrometry (GC-MS) [3]. For instance, after the bed was completely saturated and heptane was no longer adsorbing or being displaced by decane, the measured effluent concentration of heptane [3] was as low as 86% of the expected (inlet) concentration. Similarly, the effluent decane concentration was measured to be as much as 111% of the inlet concentration at

300 min, which is unlikely as there were no other adsorbates in the mixture that should be capable of displacing decane.

Initially, i.e., prior to breakthrough, both decane and heptane were completely adsorbed because there were enough active adsorption sites for both, resulting in a zero effluent concentration (Figure 3.2a). At about 75min after the start of adsorption, heptane broke through and its effluent concentration then rapidly increased beyond the inlet concentration until it reached a maximum value of 2.3 times its influent concentration (at about 143 min) because of continuous desorption due to displacement by decane from the inlet region of the bed. The deviation between the modelled and measured peaks could be due to approximation errors such as errors in determining mass transfer resistance and equilibrium parameters and /or experimental error in concentration measurements. Subsequently, the heptane effluent concentration decreased until reaching its influent concentration. Decane broke through at 152 min and continued to adsorb until the bed was completely saturated (about 248 min after the start of adsorption).

Figure 3.2b compares the amounts of decane and heptane adsorbed at the conclusion of the experiment (300 min after the start of adsorption) as given by the model and as experimentally determined. The model predicted the total amount adsorbed with a 1% MRAE compared to the experimentally determined value. The MRAE was larger for heptane (200%) than for decane (0.74%), in part since the adsorbed amount of heptane was smaller and could lead to a larger relative error. Inhomogeneity of the BAC sample may have also contributed.

Extraction was performed for a small representative sample, about 1 g, taken from the 7.16g of saturated BAC after adsorption. [3] Because heptane is preferentially found towards the outlet part of the bed at the end of adsorption, if the entire bed sample was not well mixed prior to sampling and extraction, the experimental result could underestimate the overall adsorbed amount of heptane.

The mechanism of competitive adsorption of heptane and decane can be seen in Figure 3.2c, showing the evolution of the two-dimensional adsorbed phase concentration distribution of each component in the bed at 45, 75 and 180 min after the start of adsorption. After 45 min decane was adsorbing closer to the inlet of the bed (about 15 to 25 mm from the inlet) by displacing adsorbed heptane while heptane adsorbed on the readily available adsorption sites where there was no competition from decane (about 25 to 40 mm from the inlet). In general the portion of the bed saturated with decane increased with adsorption time and heptane was continuously displaced from the region closer to the inlet by decane. After 75 min from the start of adsorption the adsorbed phase concentration distribution of heptane showed a more diffuse mass transfer zone since heptane was displaced by decane closer to the inlet and adsorbed on the unoccupied adsorption sites closer to the outlet. In contrast, decane showed a narrower mass transfer zone. After 180 min decane had almost completely displaced heptane and occupied the entire bed. Figure 3.2c also shows the velocity of mass transfer zone is higher for heptane which indicates that heptane has a higher rate of diffusion and adsorbs faster than decane. On the other hand decane was still adsorbing when heptane broke through indicating that decane has stronger affinity to the

adsorbent and adsorbed by displacing heptane which is consistent with the literature [40]. The latter point is substantiated by the values of the Langmuir affinity coefficient and the mass transfer resistance, which was higher for decane.

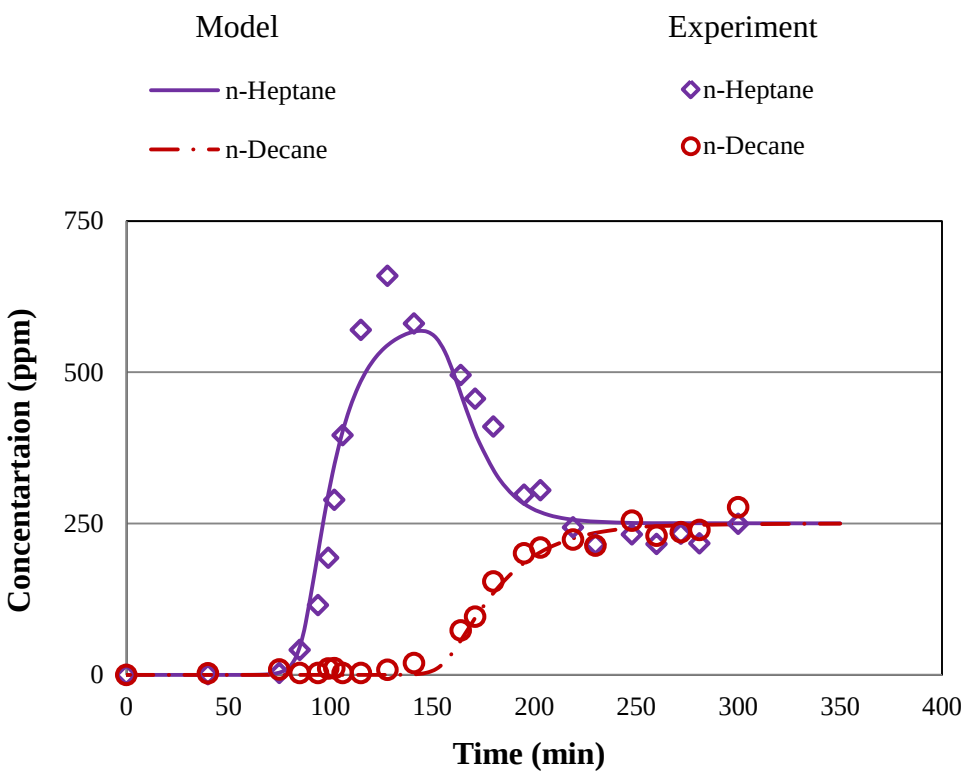
Model
Experiment
n-Heptane
n-Decane
n-Heptane
n-Decane
750
500
250
0
Concentartaion (ppm)
0
50
100
150
200
250
300
350
400
Time (min)

(a)

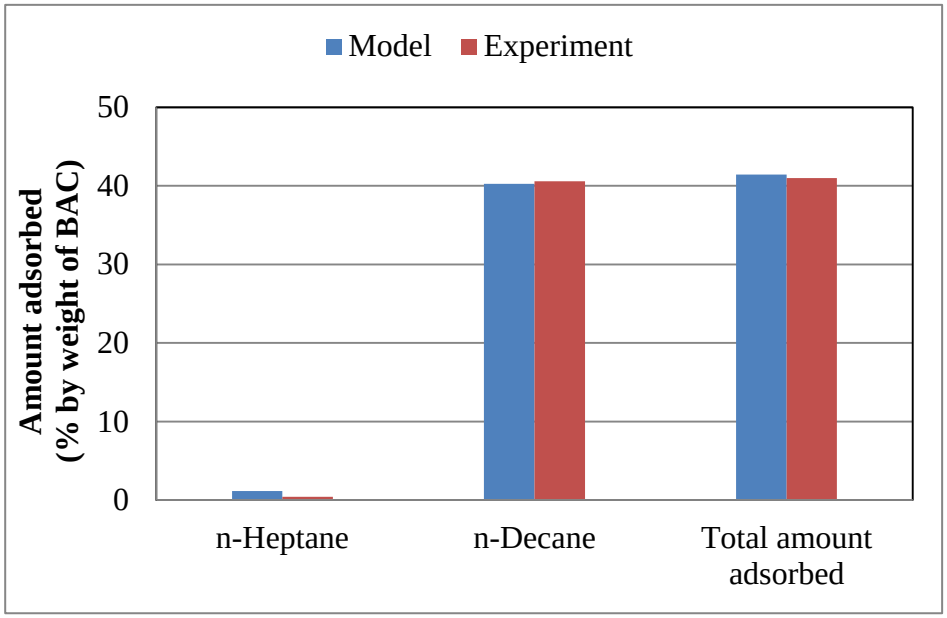
Model
Experiment
50
40
30
20
10
0
Amount adsorbed (% by weight of BAC)
n-Heptane
n-Decane
Total amount adsorbed

(b)

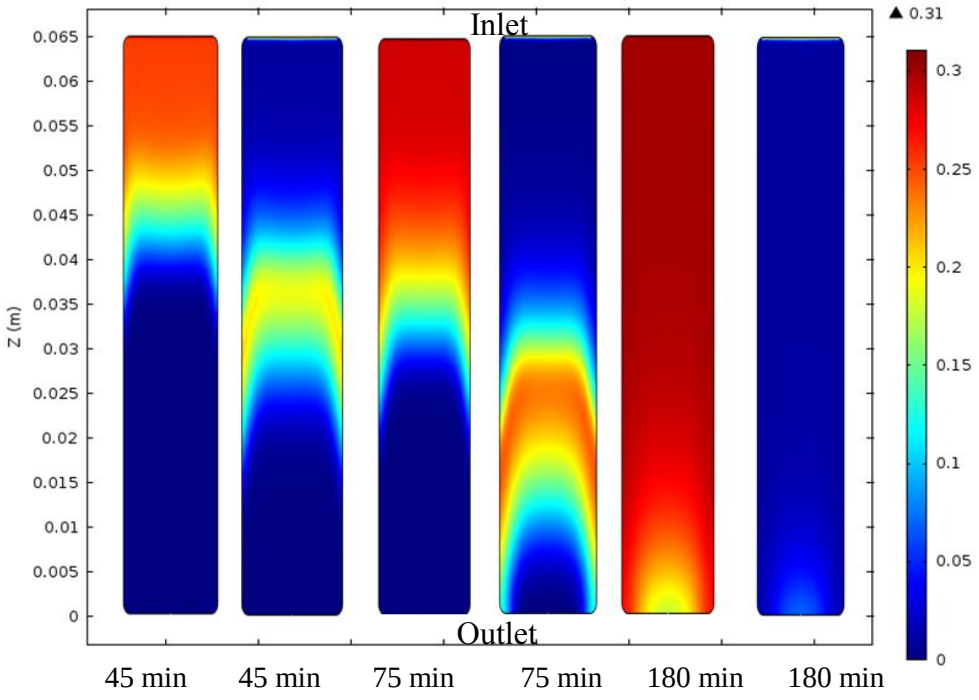

(c)

Figure 3.2. Competitive adsorption of decane and heptane (a) comparison of experimental [3] and modelled breakthrough curves, (b) comparison of amount adsorbed 300 min after the start of adsorption of each component with the measure data [3] and (c) adsorbed phase two-dimensional concentration distribution at 45, 75 and 180 min after the start of adsorption

3.4.3 Multicomponent (n=8) Adsorption

Figure 3.3a compares the modelled breakthrough curves of an eight-component VOC mixture with experimentally measured ones [3]. The mixture contained organic solvents representing different functional groups present in VOCs that are commonly present in automotive painting emissions. Detailed information about the properties of these adsorbates and the composition of the influent gas is given elsewhere [3]. The modelled and measured breakthrough curves were in good agreement as indicated by the MRAE and RMSE values of 12 and 9 %, respectively. The deviations are most likely due to experimental error [3]. For

example the effluent concentration of displaced light adsorbates such as n-butanol and n-butyl acetate should equal their influent concentration towards the end of adsorption; however, they were lower. The magnitude of experimental error is shown by the fact that the experimentally measured concentrations of most species fluctuated by up to ± 5 ppmv towards the end of adsorption. Inaccuracies of model approximation could also be reflected in the error metrics.

In the first 70 min after the start of adsorption all compounds adsorbed and the total effluent concentration was about 0.25 % of the total influent concentration. At 70 min the effluent concentration of butanol increased sharply and then reached a maximum of 121 % more than its influent concentration at about 133 min. This was followed by the breakthrough of n-butyl acetate whose effluent concentration also increased rapidly to reach a peak value of about 121 % more than its influent concentration at 144 min. This was followed by 2-heptanone and 2-butoxyethanol which showed an overshoot of 50 and 19 % respectively. The overshoot of these four compounds is attributed to the effect of concentration on the adsorbent followed by rapid displacement by more strongly adsorbing components (decane, indane, DMPB and TMB and/ or by displacing themselves as any compound with higher affinity to the adsorbent can displace the one with lower affinity. The first two components, n-butanol and n-butyl acetate, showed a very fast adsorption rate which is partly due to their higher molecular diffusivity and the enhancement of the diffusion rate by displacement by the heavier components in the mixture [41]. On the other hand, the strongly competing adsorbates (TMB, DMPB, indane and decane) had relatively diffuse breakthrough

curves and needed longer times to reach saturation. This is because these adsorbates have stronger adsorption affinities to BAC which increased their diffusion resistance and reduce their rate of diffusion. Also, these compounds both adsorb to unoccupied sites and by displacing more weakly adsorbing components.

Figure 3.3b compares the modelled and measured amounts adsorbed (by percent weight of BAC) of each component 390 min after the start of adsorption [3]. In general, there is very good agreement between the measured and the modelled values except for low molecular weight compounds. The MRAE between the modelled and experientially determined total mass adsorbed was 2.2%. The MRAE was larger for the lighter compounds possibly due to inhomogeneity in the extracted sample and/or the smaller amounts adsorbed of the lighter compounds. Wang et al. [3] reported that the amounts adsorbed based on solvent extraction of the BAC was lower than the amounts adsorbed obtained by integrating the areas above the breakthrough curves.

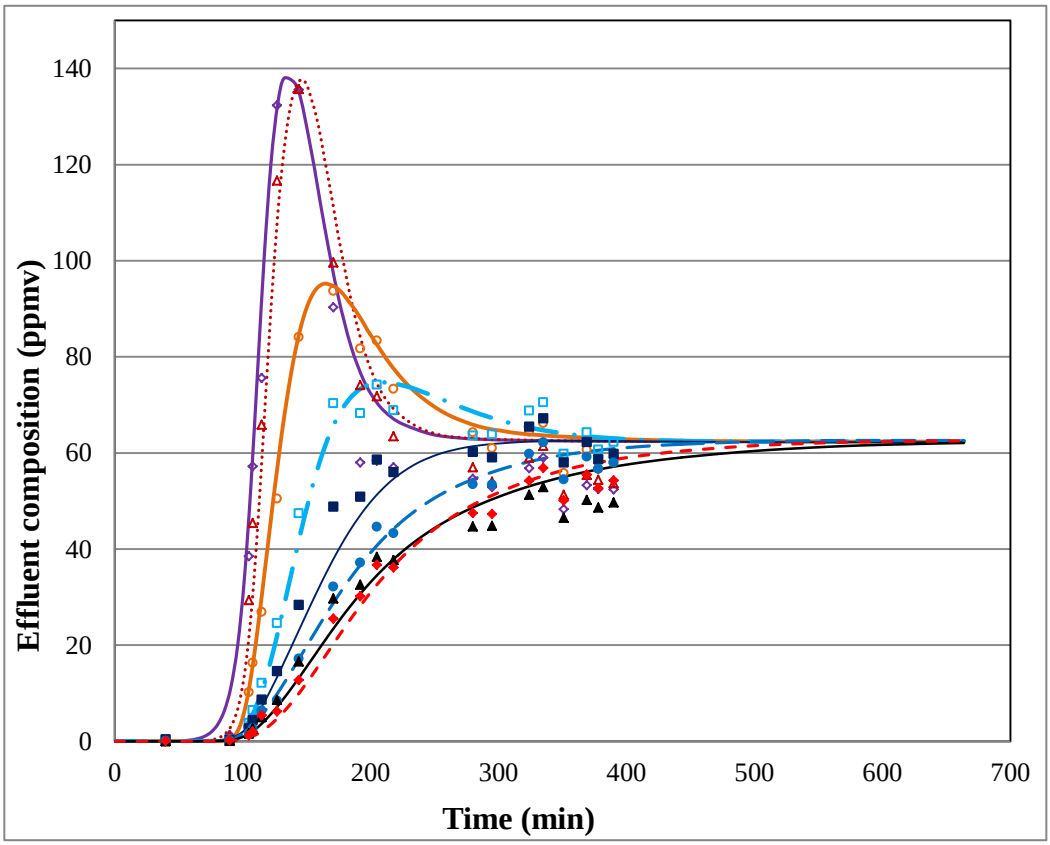
Model
Experiment
n-butanol
n-butylacetate
2-heptnone
2-butoxyethanol
decane
indan
2,2-dimethylpropylbenzene
1,2,4-trimethylbenzene
n-butanol
n-butyl acetate
2-heptanone
2-butoxyethanol
decane
indan
2,2-dimethylpropylbenzene
1,2,4-trimethylbenzene
Effluent composition (ppmv)
Time (min)
0
20
40
60
80
100
120
140
0
100
200
300
400
500
600
700

(a)

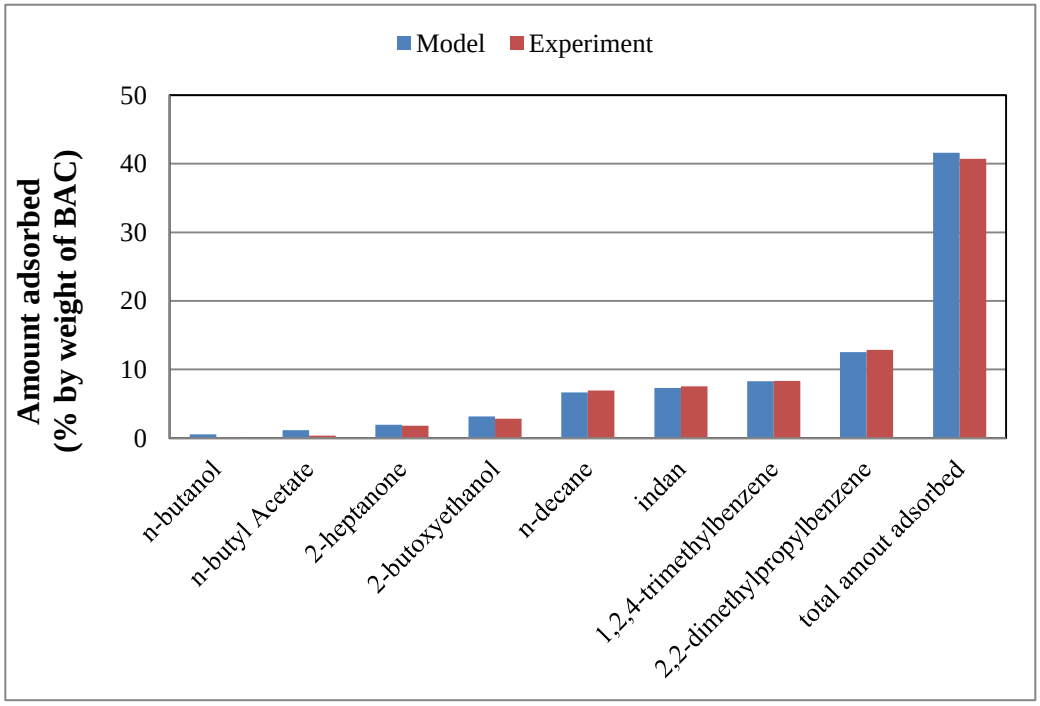

(b)

Figure 3.3 Competitive adsorption of n-butanol, n-butyl acetate, 2-heptanone, 2-butoxyethanol, decane, indane, 2, 2-dimethylpropylbenzene (DMPB), and 1, 2, 4-trimethylbenzene (TMB); (a) comparison of experimental ^{3} and modelled breakthrough curves and (b) comparison of experimental ^{3} and modelled masses adsorbed of each adsorbate 390 min after the start of adsorption

Figure 3.4 illustrates the two-dimensional adsorbed phase concentration distribution of each component of the mixture after 75 and 105 min from the start of adsorption. The inlet part of the bed is occupied with the four more strongly competing components and the adsorbed phase concentration of light components (with weaker affinity to the adsorbent) occupied the region towards the outlet of the bed. The pattern within the advancing mass transfer zone in the bed is consistent with the breakthrough of the respective components. Components with weaker affinity to the adsorbent diffused faster and occupied the adsorption sites

faster than the strongly competing ones, as indicated by the movement of their mass transfer zones. Of the eight components, n-butanol, n-butyl acetate, and 2-heptanone are the most readily displaced adsorbates and their adsorbed phase concentration showed four distinct regions in the bed from the inlet down to the outlet: where they were almost completely displaced, where they are being displaced, where their rate of adsorption dominates desorption due to displacement, and where they are adsorbing. This is consistent with the breakthrough indicated by the corresponding overshoots (Figure 3.3a) and the Langmuir affinity coefficient. The displaced adsorbates have lower affinity coefficient, heat of adsorption, mass transfer resistance relative to the corresponding displacing adsorbates. In addition, the displacement of the lighter adsorbates decreased their mass transfer resistance and resulted in their relatively sharper breakthrough curves consistent with previous experimental findings. [41, 42] On the other hand, the heavier adsorbates had a shallower breakthrough not only due to their higher mass transfer resistance but also because they adsorbed by displacing the lighter adsorbates which further retarded their mass transfer rate.

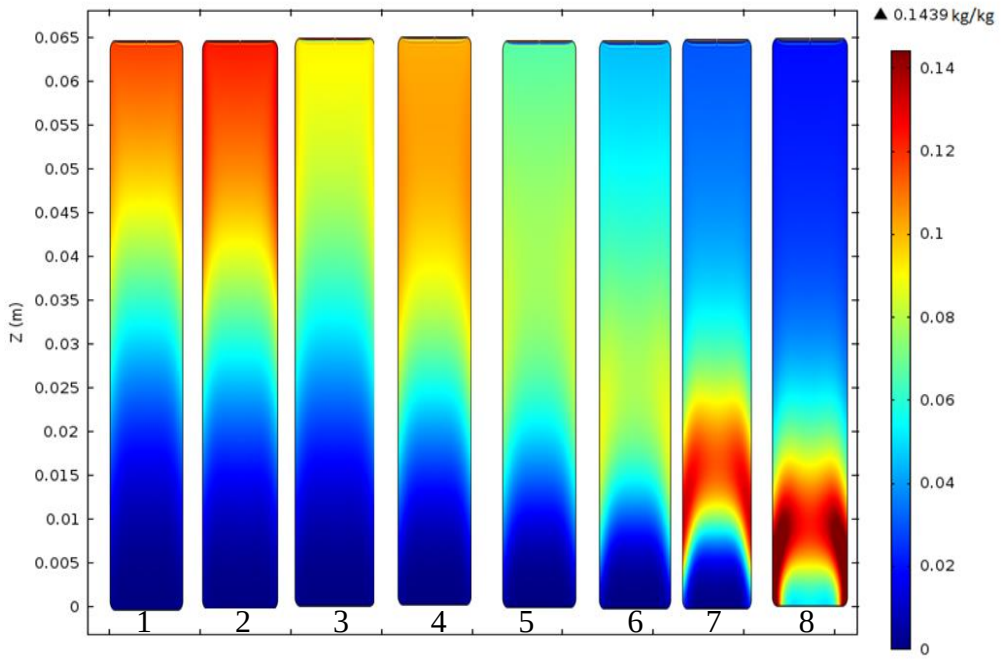

(a)

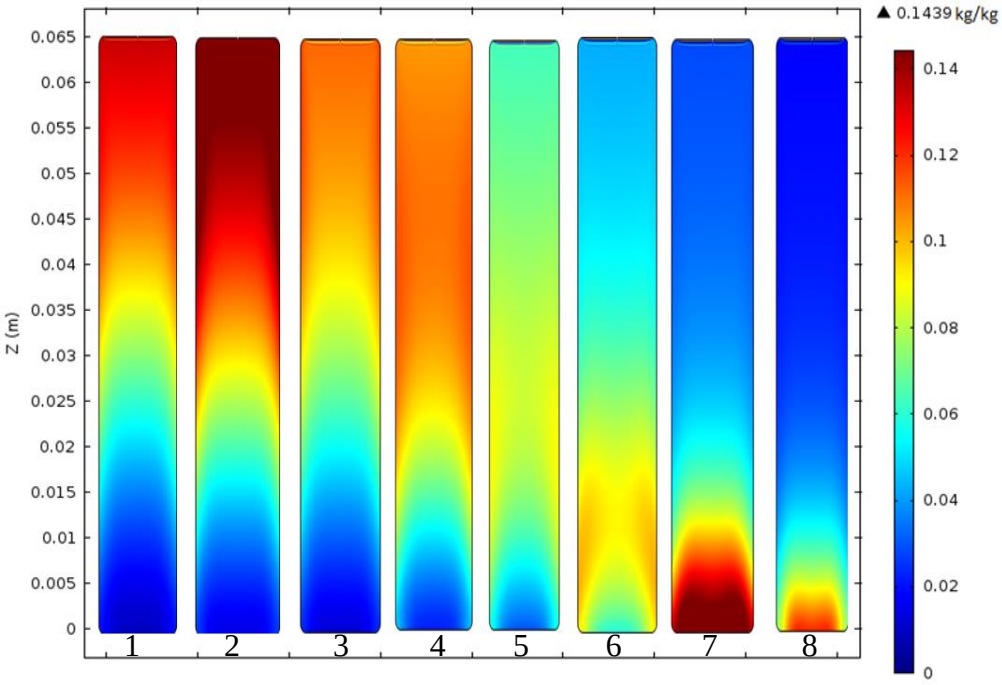

(b)

Figure 3.4. Adsorbed phase concentration distribution of 1, 2, 4-trimethylbenzene (1), 2, 2-dimethylpropylbenzene (2), indane (3), decane (4), 2-butoxyethanol (5), 2-heptanone (6) n-butyl acetate (7) and n-butanol (8), (a) 75 and (b) 105 min after the start of adsorption.

In general the model developed in this study showed promising accuracy in predicting the dynamics of competitive adsorption of VOCs from the gas stream. The model is fully predictive and theoretically could be used for the study of competitive adsorption of any n-component VOC mixture. The newly derived multicomponent competitive adsorption isotherm equation, coupled with the dynamic adsorption model, reasonably described the equilibrium adsorption of a 2- and 8-component VOC mixture. The result of the study is helpful to understand the mechanism of competitive adsorption from the gas phase.

3.5 References

1. Kim, B. R., VOC emissions from automotive painting and their control: A review. *Environmental Engineering Research* **2011,** *16*, (1), 1-9.
2. Chiang, Y. C.; Lee, C. C.; Su, W. P., Adsorption behaviors of activated carbons for the exhaust from spray painting booths in vehicle surface coating. *Toxicological & Environmental Chemistry*. **2006,** *88*, (3), 453-467.
3. Wang, H.; Jahandar Lashaki, M.; Fayaz, M.; Hashisho, Z.; Philips, J. H.; Anderson, J. E.; Nichols, M., Adsorption and desorption of mixtures of organic vapors on beaded activated carbon. *Environmental Science and Technology* **2012,** *46*, (15), 8341-8350.
4. Sexton, K.; Westberg, H., Ambient hydrocarbon and ozone measurements downwind of a large automotive painting plant. *Environmental Science and Technology* **1980,** *14*, (3), 329-332.
5. Helfferich, F. G.; Klein, G., *Multicomponent Chromatography; Theory of Interference*. M. Dekker: New York,, 1970; P viii, 419 p.
6. Lillo-Ródenas, M. A.; Fletcher, A. J.; Thomas, K. M.; Cazorla-Amorós, D.; Linares-Solano, A., Competitive adsorption of a benzene-toluene mixture on activated carbons at low concentration. *Carbon* **2006,** *44*, (8), 1455-1463.
7. Ahmed, M. J.; Mohammed, A. H. A. K.; Kadhum, A. A. H., Modeling of Breakthrough Curves for Adsorption of Propane, n-Butane, and Iso-Butane Mixture on 5A Molecular Sieve Zeolite. *Transport in Porous Media* **2011,** *86*, (1), 215-228.
8. Gironi, F.; Piemonte, V., VOCs removal from dilute vapour streams by adsorption onto activated carbon. *Chemical Engineering Journal*. **2011,** *172*, (2–3), 671-677.
9. Lu, L.; Wang, Q.; Liu, Y., Adsorption and separation of ternary and quaternary mixtures of short linear alkanes in zeolites by molecular simulation. *Langmuir* **2003,** *19*, (25), 10617-10623.
10. To, P. C.; Mariñas, B. J.; Snoeyink, V. L.; Wun, J. N., Effect of pore-blocking background compounds on the kinetics of trace organic contaminant desorption from activated carbon. *Environmental Science and Technology* **2008,** *42*, (13), 4825-4830.
11. Butler, J. A. V.; Ockrent, C., Studies in electrocapillarity. Part III: The surface tensions of solutions containing two surface-active solutes. *Journal of Physical Chemistry.* **1930,** *34*, (12), 2841-2859.
12. Do, D. D., *Adsorption analysi : Equilibria and Kinetics*. Imperial College Press: London, 2008; Vol. v 2.
13. Toth, J., *Adsorption: Theory, Modeling, and Analysis* Marcel Dekker.Inc: New York, 2002; Vol. 107.
14. Jain, J. S.; Snoeyink, V. L., Adsorption from bisolute systems on active carbon. *Journal of the Water Pollution Control Federation* **1973,** *45*, (12), 2463-2479.

15. Alkhamis, K. A.; Wurster, D. E., Prediction of adsorption from multicomponent solutions by activated carbon using single-solute parameters. Part II - Proposed equation. *AAPS PharmSciTech* **2002,** *3*, (3).
16. Dereje Tamiru Tefera, M. J. L., Mohammadreza Fayaz , John H. Philips, James E. Anderson, Mark Nichols,Zaher Hashisho, Two-Dimensional Modeling of Volatile Organic Compounds Adsorption onto Beaded Activated Carbon. In *Environmental Science & Technology*, 2013.
17. Giraudet, S.; Pré, P.; Le Cloirec, P., Modeling the heat and mass transfers in temperature-swing adsorption of volatile organic compounds onto activated carbons. *Environmental Science and Technology* **2009,** *43*, (4), 1173-1179.
18. Joly, A.; Perrard, A., Linear driving force models for dynamic adsorption of volatile organic compound traces by porous adsorbent beds. *Mathematics and Computers in Simulation* **2009,** *79*, (12), 3492-3499.
19. Giraudet, S.; Pŕ, P.; Le Cloirec, P., Modeling the temperature dependence of adsorption equilibriums of VOC(s) onto activated carbons. *Journal of Environmental Engineering* **2010,** *136*, (1), 103-111.
20. Nield, D. A.; Bejan, A. Nield, D.A; Bejan. A. *Convection in Porous Media*; Springer: New York, 2006.
21. Smith, J. M.; Van Ness, H. C.; Abbott, M. M., *Introduction to Chemical Engineering thermodynamics*. 7th ed.; McGraw-Hill: Boston, 2005; p xviii, 817 p.
22. Bowen, D. H. M., HIST 15-Perry's Heavyweight Handbook for Chemical Engineers. *Abstracts of Papers of the American Chemical Society* **2008,** *236*.
23. Logan, D. A., Estimating physical properties for control equipment design. *Environmental Progress* **1997,** *16*, (4), 237-242.
24. Cohen, Y.; Metzner, A. B., Wall effects in laminar flow of fluids through packed beds. *AIChE Journal* **1981,** *27*, (5), 705-715.
25. Mu, D.; Liu, Z. S.; Huang, C.; Djilali, N., Determination of the effective diffusion coefficient in porous media including Knudsen effects. *Microfluidics and Nanofluidics* **2008,** *4*, (3), 257-260.
26. Shi, Y.; Lee, Y. T.; Kim, A. S., Knudsen Diffusion Through Cylindrical Tubes of Varying Radii: Theory and Monte Carlo Simulations. *Transport in Porous Media* **2012,** *93*, (3), 517-541.
27. Lashaki, M. J.; Fayaz, M.; Wang, H.; Hashisho, Z.; Philips, J. H.; Anderson, J. E.; Nichols, M., Effect of adsorption and regeneration temperature on irreversible adsorption of organic vapors on beaded activated carbon. *Environmental Science and Technology* **2012,** *46*, (7), 4083-4090.
28. Dantas, T. L. P.; Luna, F. M. T.; Silva Jr, I. J.; Torres, A. E. B.; De Azevedo, D. C. S.; Rodrigues, A. E.; Moreira, R. F. P. M., Modeling of the fixed-bed adsorption of carbon dioxide and a carbon dioxidenitrogen mixture on zeolite 13X. *Brazilian Journal of Chemical Engineering* **2011,** *28*, (3), 533-544.
29. Giraudet, S.; Pré, P.; Tezel, H.; Le Cloirec, P., Estimation of adsorption energies using the physical characteristics of activated carbons and the

molecular properties of volatile organic compounds. *Carbon* **2006,** *44*, (12), 2413-2421.
30. Kwapinski, W., Combined wall and thermal effects during non-isothermal packed bed adsorption. *Chemical Engineering Journal* **2009,** *152*, (1), 271-276.
31. Kannuluik, W. G.; Carman, E. H., The Temperature Dependence of the Thermal Conductivity of Air. *Australian Journal of Scientific Research Series A-Physical Sciences* **1951,** *4*, (3), 305-314.
32. Kuwagaki, H.; Meguro, T.; Tatami, J.; Komeya, K.; Tamura, K., An improvement of thermal conduction of activated carbon by adding graphite. *Journal of Materials Science* **2003,** *38*, (15), 3279-3284.
33. Bey, O.; Eigenberger, G., Gas flow and heat transfer through catalyst filled tubes. *International Journal of Thermal Sciences* **2001,** *40*, (2), 152-164.
34. Guo, P., Dependency of Tortuosity and Permeability of Porous Media on Directional Distribution of Pore Voids. *Transport in Porous Media* **2012,** *95*, (2), 285-303.
35. Oberkampf, W. L.; Trucano, T. G., Verification and validation in computational fluid dynamics. *Progress in Aerospace Sciences* **2002,** *38*, (3), 209-272.
36. Hutton, A. G., Quality and trust in industrial computational fluid dynamics. Houille Blanche **2001**, (3-4), 25-28.
37. Oliemans, R. V. A., ERCOFTAC's role in promoting computational fluid dynamics. *Houille Blanche* **2000**, (7-8), 43-46.
38. Jahandar Lashaki, M.; Fayaz, M.; Niknaddaf, S.; Hashisho, Z., Effect of the adsorbate kinetic diameter on the accuracy of the Dubinin-Radushkevich equation for modeling adsorption of organic vapors on activated carbon. *Journal of Hazardous Materials* **2012,** *241-242*, 154-163.
39. Williams, L. E.; Barnett, M. O.; Kramer, T. A.; Melville, J. G., Adsorption and transport of arsenic(V) in experimental subsurface systems. *Journal of Environmental Quality* **2003,** *32*, (3), 841-850.
40. Sulaymon, A. H.; Ahmed, K. W., Competitive adsorption of furfural and phenolic compounds onto activated carbon in fixed bed column. *Environmental Science and Technology* **2008,** *42*, (2), 392-397.
41. To, P. C.; Mariñas, B. J.; Snoeyink, V. L.; Wun, J. N., Effect of strongly competing background compounds on the kinetics of trace organic contaminant desorption from activated carbon. *Environmental Science and Technology* **2008,** *42*, (7), 2606-2611.
42. Pelekani, C.; Snoeyink, V. L., Kinetic and equilibrium study of competitive adsorption between atrazine and Congo red dye on activated carbon: The importance of pore size distribution. *Carbon* **2001,** *39*, (1), 25-37.

CHAPTER 4 CONCLUSION AND RECOMMENDATION

4.1 Conclusion

This research set out to develop a fully predictive and accurate two dimensional mathematical model to investigate adsorption of volatile organic compounds from diluted gaseous stream in a fixed bed adsorber. This research is important because it contributes to the understanding of the mechanism of adsorption of single and multicomponent VOCs from diluted gas streams. The model developed in this study could be used to facilitate the design and optimization of the fixed bed adsorber and reduces the number of pilot scale testes required to measure the effect of various operation and design variables.

The first part (chapter two) of the research concentrated on the development and simulation of a 2D single component VOC adsorption model. The model was validated for different VOCs selected based on their molecular weight, boiling point and affinity to the adsorbent in order to ensure the accuracy of the model for the adsorption of a range of VOCs emitted from automotive painting operations. The model was validated for effluent concentration, pressure and temperature with experimentally measured data from a bench-scale fixed bed adsorber. The deviation of the model result from the measured effluent concentration, pressure and temperature, as measured by the relative mean relative absolute error (MRAE) was 2.6, 11.8 and 1.1% respectively indicating that the model has comparable accuracy to the experimental tests and could be used to reduce the number of experiments needed. To complete the validation of the single component model, the response of the model to changes in the adsorber's operation condition (carrier gas temperature, adsorbate loading, superficial

velocity) and adsorbent property (particle size) was investigated. The model was found to be sensitive to changes to the operation conditions and adsorbent particle size and the response of the model was consistent with earlier experimental studies. The major conclusions of the parametric study are the following:

- As the adsorbate loading increases, the bed temperature increases,
- As the carrier gas temperature increases, the breakthrough time decreases,
- As the superficial velocity increases, the breakthrough time decreases and the breakthrough become more diffused,
- As the particle size decreases, the breakthrough become sharper indicating enhanced mass transfer rate.

The second part of this research focused on the modeling of competitive adsorption of n-component mixture of VOCs from dilute gas streams. This was done by extending the validated single component dynamic adsorption model (chapter 2) to predict competitive adsorption of mixture of adsorbates and deriving a new competitive adsorption isotherm model. The model was validated using published (breakthrough curve and total amount adsorbed) data on the competitive adsorption of binary and an eight component mixtures of VOCs. For the binary and eight-component mixtures, the MRAE of the breakthrough profiles was 13 and 12%, respectively while the MRAE of the adsorbed amounts was 1 and 2%, respectively which confirms the accuracy of the model to predict competitive adsorption of mixture of VOCs. This study is important because it enhance the understanding of competitive adsorption of mixture of VOCs regardless of the number of adsorbates involved which was not available in

previous studies. The major conclusions from study of competitive adsorption are summarized as follows:

- During initial stage of the adsorption of mixture of VOCs onto BAC there is abundant adsorption sites, thus strongly adsorbing as well as weakly adsorbing components can readily adsorb onto vacant adsorption sites though there is still competition. However, as adsorption time increases the inlet region of the bed is dominated by strongly adsorbing components. This is because adsorbates with higher affinity adsorbed by displacing weakly adsorbed components. The weakly adsorbing components (relatively faster mass transfer rate) on the other hand move ahead with the bulk fluid and occupy the fresh adsorption sites first in the front part of the bed. This process continues until the mass transfer zone of the lighter components reach the outlet region of the bed. After that adsorbates with higher affinity continue to adsorb by displacing the weakly adsorbed components until they occupy the whole region of the bed. As a result the large portion of the adsorbed phase concentration consists of the heavier or strongly adsorbing components as the adsorption time increases. The effluent concentrations of weakly adsorbing components sharply increase, once they breakthrough, to a value above their inlet concentration because they are displaced from the adsorbed phase.

- The competition of the components for the adsorption sites could be related to heat of adsorption, affinity coefficient, and mass transfer resistance as follows:
    - The higher is the affinity coefficient the stronger is the competition of the component, i.e. components with higher affinity coefficients displace components with lower affinity coefficients.
    - The higher is the mass transfer resistance the higher is the competition of the adsorbate. This is because the mass transfer resistance itself depends on the affinity of the adsorbate (adsorbent-adsorbate interaction), hence the higher is the affinity of the adsorbate for the adsorbent the more strongly it adsorbs and the higher is the pore or surface diffusion of the adsorbate.
    - The higher is the heat of adsorption the higher is the competition of the adsorbate for adsorption sites. The stronger is the adsorbate adsorbent interaction the higher is the heat of adsorption.

4.2 Recommendation for Future Work

The research completed for this thesis has highlighted a number of topics that needs further research. The major research areas are:

- The effect of carrier gas moisture on the adsorption of VOCs. The general understanding in the existing literature is that the presence of moisture can reduce the adsorption capacity of activated carbon for VOCs, particularly

for polar ones. Hence, accurate analysis of the effect of moisture on adsorption of VOCs should be investigated.

- In order to offset the effect of moisture on the adsorption of VOCs onto activated carbon some industries increase the adsorption temperature. However, the higher is the adsorption temperature the lower is the adsorption capacity of the adsorbent to the adsorbate. The model developed in this study could be modified to account for the effect of temperature on the moisture content and adsorption of water vapor and VOCs. Hence the model can help in finding the optimum adsorption temperature.
- The model could be modified to simulate the desorption process following VOC(s) adsorption. This could be very helpful to investigate the most important parameters affecting the process of regeneration.
- Another immediate research topic is the modelling of different adsorber configurations such as fluidized bed, moving bed etc. This could be helpful in selection of the best adsorber configuration for a particular VOC adsorption application.

CHAPTER 5 APPENDICES

APPENDIX A Derivation of Isotherm Equation for Competitive Adsorption

APPENDIX B Physical Properties of the Adsorbates

APPENDIX A Derivation of Isotherm Equation for Competitive Adsorption

Single component Langmuir isotherm model was extended by Butler and Ockrent [1] to predict competitive adsorption of mixture of binary component until Jain and Snoeyink [2] revealed the limitation of the former extension of single component Langmuir isotherm to competitive adsorption of binary system and proposed a new form of competitive isotherm for binary mixture of organic compounds from wastewater (equation A1 and A2) wherein (q_{m1}>q_{m2}) [3].

$$q_1=\frac{(q_{m1}-q_{m2})b_1C_1}{1+b_1C_1}+\frac{q_{m2}b_1C_1}{1+b_1C_1+b_2C_2} \quad \text{A1}$$

$$q_2=\frac{q_{m2}b_2C_2}{1+b_1C_1+b_2C_2} \quad \text{A2}$$

The model for adsorption competing binary mixture was then modified for the prediction of ternary ($q_{m1} > q_{m2} > q_{m3}$) mixture from an aqueous system [4].

$$q_1=\frac{(q_{m1\_}q_{m2})b_1C_1}{1+b_1C_1}+\frac{(q_{m2\_}q_{m3})b_1C_1}{1+b_1C_1+b_2C_2}+\frac{q_{m3}b_1C_1}{1+b_1C_1+b_2C_2+b_3C_3} \quad \text{A3}$$

$$q_2=\frac{(q_{m2\_}q_{m3})b_2C_2}{1+b_1C_1+b_2C_2}+\frac{q_{m3}b_2C_2}{1+b_1C_1+b_2C_2+b_3C_3} \quad \text{A4}$$

$$q_3=\frac{q_{m3}b_3C_3}{1+b_1C_1+b_2C_2+b_3C_3} \quad \text{A5}$$

General isotherm equation for ith component adsorbate

In the current study, the model for competitive adsorption of ternary system was extended for n-component mixture of VOCs for adsorption from a gas stream and tested with an eight-component VOCs mixture in which $(q_{m1} > q_{m2} > q_{m3} > q_{m4} > \cdots \ldots \ldots \ldots \ldots \ldots > q_{m7} > q_{m8})$.

$$q_1 = \frac{(q_{m1-}q_{m2})b_1C_1}{1+b_1C_1} + \frac{(q_{m2-}q_{m3})b_1C_1}{1+b_1C_1+b_2C_2} + \frac{(q_{m3}-q_{m4})b_1C_1}{1+b_1C_1+b_2C_2+b_3C_3} + \frac{(q_{m4}-q_{m5})b_1C_1}{1+b_1C_1+b_2C_2+b_3C_3+b_4C_4} +$$

$$\frac{(q_{m5}-q_{m6})b_1C_1}{1+b_1C_1+b_2C_2+b_3C_3+b_4C_{4+}\ b_5C_5} +$$

$$\frac{(q_{m6}-q_{m7})b_1C_1}{1+b_1C_1+b_2C_2+b_3C_3+b_4C_4+b_5C_{5+}b_6C_6} + \frac{(q_{m7-}\ q_{m8})b_1C_1}{1+b_1C_1+b_2C_2+b_3C_3+b_4C_4+b_5C_{5+}b_6C_6+b_7C_7} +$$

$$\frac{q_{m8}b_1C_1}{1+b_1C_1+b_2C_2+b_3C_3+b_4C_4+b_5C_{5+}b_6C_6+b_7C_7+b_8C_8} \quad \text{A6}$$

$$q_2 =$$

$$\frac{(q_{m2-}q_{m3})b_2C_2}{1+b_1C_1+b_2C_2} + \frac{(q_{m3}-q_{m4})b_2C_2}{1+b_1C_1+b_2C_2+b_3C_3} + \frac{(q_{m4}-q_{m5})b_2C_2}{1+b_1C_1+b_2C_2+b_3C_3+b_4C_4} +$$

$$\frac{(q_{m5}-q_{m6})b_1C_1}{1+b_1C_1+b_2C_2+b_3C_3+b_4C_{4+}\ b_5C_5} +$$

$$\frac{(q_{m6}-q_{m7})b_2C_2}{1+b_1C_1+b_2C_2+b_3C_3+b_4C_4+b_5C_{5+}b_6C_6} + \frac{(q_{m7-}\ q_{m8})b_2C_2}{1+b_1C_1+b_2C_2+b_3C_3+b_4C_4+b_5C_{5+}b_6C_6+b_7C_7} +$$

$$\frac{q_{m8}b_2C_2}{1+b_1C_1+b_2C_2+b_3C_3+b_4C_4+b_5C_{5+}b_6C_6+b_7C_7+b_8C_8} \quad \text{A7}$$

$$q_3 = \frac{(q_{m3}-q_{m4})b_3C_3}{1+b_1C_1+b_2C_2+b_3C_3} + \frac{(q_{m4}-q_{m5})b_3C_3}{1+b_1C_1+b_2C_2+b_3C_3+b_4C_4} + \frac{(q_{m5}-q_{m6})b_3C_3}{1+b_1C_1+b_2C_2+b_3C_3+b_4C_{4+}\ b_5C_5}$$

$$+\frac{(q_{m6}-q_{m7})b_3C_3}{1+b_1C_1+b_2C_2+b_3C_3+b_4C_4+b_5C_{5+}b_6C_6} + \frac{(q_{m7-}\ q_{m8})b_3C_3}{1+b_1C_1+b_2C_2+b_3C_3+b_4C_4+b_5C_{5+}b_6C_6+b_7C_7} +$$

$$\frac{q_{m8}b_3C_3}{1+b_1C_1+b_2C_2+b_3C_3+b_4C_4+b_5C_{5+}b_6C_6+b_7C_7+b_8C_8} \quad \text{A8}$$

$$q_4 = \frac{(q_{m4}-q_{m5})b_4C_4}{1+b_1C_1+b_2C_2+b_3C_3+b_4C_4} + \frac{(q_{m5}-q_{m6})b_4C_4}{1+b_1C_1+b_2C_2+b_3C_3+b_4C_{4+}\ b_5C_5}$$

$$+\frac{(q_{m6}-q_{m7})b_4C_4}{1+b_1C_1+b_2C_2+b_3C_3+b_4C_4+b_5C_5+b_6C_6} + \frac{(q_{m7-}\ q_{m8})b_4C_4}{1+b_1C_1+b_2C_2+b_3C_3+b_4C_4+b_5C_5+b_6C_6+b_7C_7} +$$

$$\frac{q_{m8}b_4C_4}{1+b_1C_1+b_2C_2+b_3C_3+b_4C_4+b_5C_5+b_6C_6+b_7C_7+b_8C_8} \quad \text{A9}$$

$$q_5 = \frac{(q_{m5}-q_{m6})b_5C_5}{1+b_1C_1+b_2C_2+b_3C_3+b_4C_{4+}\ b_5C_5} + \frac{(q_{m6}-q_{m7})b_5C_5}{1+b_1C_1+b_2C_2+b_3C_3+b_4C_4+b_5C_5+b_6C_6} +$$

$$\frac{(q_{m7-}\ q_{m8})b_5C_5}{1+b_1C_1+b_2C_2+b_3C_3+b_4C_4+b_5C_5+b_6C_6+b_7C_7} +$$

$$\frac{q_{m8}b_5C_5}{1+b_1C_1+b_2C_2+b_3C_3+b_4C_4+b_5C_5+b_6C_6+b_7C_7+b_8C_8} \quad \text{A10}$$

$$q_6 = \frac{(q_{m6}-q_{m7})b_6C_6}{1+b_1C_1+b_2C_2+b_3C_3+b_4C_4+b_5C_5+b_6C_6} + \frac{(q_{m7-}\ q_{m8})b_6C_6}{1+b_1C_1+b_2C_2+b_3C_3+b_4C_4+b_5C_5+b_6C_6+b_7C_7} +$$

$$\frac{q_{m8}b_6C_6}{1+b_1C_1+b_2C_2+b_3C_3+b_4C_4+b_5C_5+b_6C_6+b_7C_7+b_8C_8} \quad \text{A11}$$

$$q_7 = \frac{(q_{m7-}\ q_{m8})b_7C_7}{1+b_1C_1+b_2C_2+b_3C_3+b_4C_4+b_5C_5+b_6C_6+b_7C_7} +$$

$$\frac{q_{m8}b_7C_7}{1+b_1C_1+b_2C_2+b_3C_3+b_4C_4+b_5C_5+b_6C_6+b_7C_7+b_8C_8} \quad \text{A12}$$

$$q_8 = \frac{q_{m8}b_8C_8}{1+b_1C_1+b_2C_2+b_3C_3+b_4C_4+b_5C_5+b_6C_6+b_7C_7+b_8C_8} \quad \text{A13}$$

The general form for the competitive adsorption isotherm equation for the i^{th} adsorbate in a mixture of n VOCs could then be written as:

$$q_i = \sum_{k=i}^{n} \frac{b_i c_i a_k}{1+\sum_{j=1}^{k} b_j c_j}:$$ A14

Where:

a_k=$(q_{m,k} - q_{m,k+1})$ for k= i to n-1

and $a_k = q_{m,n}$, for k = n

APPENDIX B Physical Properties of the Adsorbates

Table B. 1 shows the physical properties of the adsorbates studied.

Table B. 1. Physical properties of the adsorbates

Compound	$M_{A,i}$ [5] (g/mol)	$\left(\sum v\right)_{A,i}$	ΔH_{vap} [6, 7] (kJ/mol)	α [8, 9] ($10^{-24}cm^3$)	γ [6, 8-10] (mN/m)	IP [8, 9, 10] (eV)
Butanol	74.10	91.28	43.29	8.71	25.57	10.14
n-Butyl acetate	116.20	133.72	36.14	12.61	24.35	10.10
Heptane	100.21	147.18	36.66	13.60	20.14	9.90
2-Heptanone	114.20	148.70	39.5	13.51	24.80	9.37
2-Butoxyethanol	118.20	137.68	47.06	13.00	27.40	10.00
n-Decane	142.30	168.3	38.75	19.10	23.90	10.20
1,2,4-trimethybenze	120.20	152.06	39.2	15.87	28.70	8.27
Indane	118.20	127.90	49.05	15.48	27.50	8.40
2,2-Dimethylpropylbenzene	148.20	192.98	46.74	19.59	28.80	7.71

References:

1. Butler, J. A. V.; Ockrent, C., Studies in electrocapillarity. Part III: The surface tensions of solutions containing two surface-active solutes. *Journal of Physical chemistry* **1930,** *34*, (12), 2841-2859.
2. Jain, J. S.; Snoeyink, V. L., Adsorption from bisolute systems on active carbon. *Journal of the Water Pollution Control Federation* **1973,** *45*, (12), 2463-2479.
3. Jain, J. S.; Vernon, L. S., Adsorption from Bisolute Systems on Active Carbon. *Journal (Water Pollution Control Federation)* **1973,** *45*, (12), 2463-2479.
4. Alkhamis, K. A.; Wurster, D. E., Prediction of adsorption from multicomponent solutions by activated carbon using single-solute parameters. Part II--Proposed equation. *AAPS PharmSciTech* **2002,** *3*, (3), E23.
5. Wang, H.; Jahandar Lashaki, M.; Fayaz, M.; Hashisho, Z.; Philips, J. H.; Anderson, J. E.; Nichols, M., Adsorption and desorption of mixtures of organic vapors on beaded activated carbon. *Environmental Science and Technology* **2012,** *46*, (15), 8341-8350.
6. Bowen, D. H. M., HIST 15-Perry's heavyweight handbook for chemical engineers. *Abstracts of Papers of the American Chemical Society* **2008,** *236*.
7. Smith, J. M.; Van Ness, H. C.; Abbott, M. M., *Introduction to Chemical Engineering Thermodynamics*. 7th ed.; McGraw-Hill: Boston, 2005; p xviii, 817 p.
8. Lide, D. R., *CRC Handbook of Chemistry and Physics*. 89th edition; Lide, D.R., Ed; CRC Press: Boca Raton, FL, 2008.
9. Ullmann, F., Ullmann's Encyclopedia of Industrial Chemistry. In VCH: Weinheim: Germany, 1985; Vol. 40 .
10. Giraudet, S.; Pré, P.; Tezel, H.; Le Cloirec, P., Estimation of adsorption energies using the physical characteristics of activated carbons and the molecular properties of volatile organic compounds. *Carbon* **2006,** *44*, (12), 2413-2421.